The Astrophysical Journal, 591:968–985, 2003 July 10

LABORATORY INFRARED SPECTROSCOPY OF CATIONIC POLYCYCLIC AROMATIC HYDROCARBON MOLECULES

Jos Oomens,[1] A. G. G. M. Tielens,[2] Boris G. Sartakov,[1,3] Gert von Helden,[1] and Gerard Meijer[1,4,5]

Received 2003 January 17; accepted 2003 March 24

ABSTRACT

Infrared spectroscopy of a variety of interstellar sources shows strong mid-IR emission bands, which are generally attributed to emission from highly vibrationally excited polycyclic aromatic hydrocarbon molecules (PAHs) in the neutral and, particularly, cationic states. Over the past decade, various experimental methods have been developed to record the infrared spectra of cationic PAHs in the laboratory. In this paper, we discuss available experimental spectra obtained with matrix isolation spectroscopy (MIS), infrared multiple-photon dissociation of trapped ions (MPD), dissociation spectroscopy of ionic PAH van der Waals clusters (VDW), and infrared emission (IRE). Moreover, we compare these experimental spectra to density functional theory (DFT) calculations. The main body of experimental data relies on MIS and MPD spectra, and we present a detailed comparison of results from these methods, providing linear and multiple-photon absorption data, respectively. The effects of multiple-photon absorption, as encountered in MPD, and multiple-photon emission, occurring in interstellar spectra, are carefully assessed with the use of mathematical models, which include the effects of vibrational anharmonicity. We show that an analysis of the multiple-photon and linear data can provide important information on the anharmonicity parameters, which is otherwise difficult to attain. This is illustrated with a detailed comparison of the linear and multiple-photon absorption spectra of the naphthalene cation, yielding experimental anharmonicity parameters for the IR-active modes in the 500–1700 cm^{-1} range.

Subject headings: astrochemistry — infrared: ISM — ISM: molecules — methods: laboratory — molecular data — techniques: spectroscopic

1. INTRODUCTION

In the early 1970s, the first spectra of some of the (necessarily) brightest infrared sources revealed the presence of unexpected strong emission features at 3.3, 6.2, 7.7, and 8.6 μm (Gillett, Forrest, & Merrill 1973; Russell, Soifer, & Willner 1977; Willner et al. 1977). Since then, ground-based, airborne, and space-based observations have shown that these features dominate the spectra of almost all objects, including H II regions, reflection nebulae, young stellar objects, planetary nebulae, post-AGB objects, the general interstellar medium of the Milky Way and other galaxies, galactic nuclei, and starburst galaxies (Verstraete et al. 1996, 2001; Moutou et al. 1999; Joblin et al. 2000; Genzel et al. 1998; Henning et al. 1998; Boulanger et al. 1998; Mattila et al. 1996; Mattila, Lehtinen, & Lemke 1999; van Kerckhoven et al. 2000; Hony et al. 2001; Peeters et al. 2002). Analysis of these data has revealed the incredible richness of the interstellar infrared features. In particular, these well-known major features are accompanied in many sources by a plethora of weaker features at 3.4, 3.5, 5.2, 5.6, 6.9, 12.7, 13.5, and 14.2 μm. Also, on closer inspection, many features show substructure and weak shoulders (Moutou et al. 1999; Peeters et al. 2002). These spectral details vary from source to source and even within sources. The overall picture emanating from these data is that these features are carried by a family of species whose detailed composition and characteristics vary depending on the local physical conditions. It is now well established that these IR emission features are due to the vibrational relaxation of UV-pumped polycyclic aromatic hydrocarbon molecules (PAHs) with sizes in the range 20–100 C atoms (Léger & Puget 1984; Allamandola, Tielens, & Barker 1985, 1989; Schutte, Tielens, & Allamandola 1993). However, the actual identification of specific molecules within this class of species has remained enigmatic. To a large extent, this may reflect that the carriers are likely to be ions and/or radicals (Allamandola et al. 1985; Bakes, Tielens, & Bauschilcher 2001a; Bakes et al. 2001b; Draine & Li 2001), i.e., species whose spectra are difficult to measure in the laboratory. This quest for the identification of the ultimate "grand PAH" has lead to vigorous laboratory efforts by a number of groups using a variety of techniques. Most of these studies have concentrated on matrix isolation techniques in which the species is isolated in an inert matrix at low temperature and the spectrum is measured in absorption (Szczepanski et al. 1992; Hudgins & Allamandola 1995a; Moutou, Léger, & d'Hendecourt 1996). Some studies have been performed in the gas phase, again in absorption (Flickinger, Wdowiak, & Gomez 1991; Colangeli et al. 1992; Joblin et al. 1995). Also, a concerted effort has been made to measure absorption spectra of PAHs based on mass spectrometry of cation fragments (Piest, von Helden, & Meijer 1999; Oomens et al. 2000). Moreover, rapid advances in computational power now allow quantum chemical studies of the vibrational properties of increasingly larger PAHs in various charge states and radical forms (DeFrees et al. 1993; Langhoff 1996; Bauschlicher, Hudgins, & Allamandola 1999; Bauschlicher & Bakes 2000;

[1] FOM Institute for Plasma Physics "Rijnhuizen," Edisonbaan 14, 3439 MN Nieuwegein, Netherlands.
[2] Kapteyn Institute, University of Groningen, Landleven 12, 9747 AD Groningen, Netherlands.
[3] General Physics Institute, Vavilov Street, Moscow, Russia.
[4] Department of Molecular and Laser Physics, University of Nijmegen, Toernooiveld 1, 6525 ED Nijmegen, Netherlands.
[5] Fritz-Haber-Institut der Max-Planck-Gesellschaft, Faradayweg 4-6, D-14195 Berlin, Germany.

Bauschlicher 2002). With this wealth of experimental and theoretical data, it has become important to critically compare the results obtained with these different techniques and assess their inherent accuracy.

A number of detailed models have been developed over the last decade to study the emission spectrum of interstellar PAHs with varying degrees of sophistication. Generally, these models are based on linear absorption spectra; that is, the emission spectrum of a species is assumed to be given by the absorption spectrum—generally measured at 10 K—multiplied by the Planck function at the instantaneous temperature of the cooling species (Léger et al. 1989; Schutte et al. 1993; Bakes et al. 2001a, 2001b; Draine & Li 2001). However, linear absorption spectroscopy is only a first approximation for the emission spectrum from highly vibrationally excited species because of the importance of anharmonic interactions (Barker, Allamandola, & Tielens 1987; Pech, Joblin, & Boissel 2002). Anharmonic coupling between modes will lead to a general redshift and asymmetric broadening of the emission bands from such species. Moreover, "hot band" ($v = 2 \rightarrow 1$) transitions will generally be displaced toward the red from the ground-state transition. Experimental studies have shown that these effects can be substantial for PAHs (Joblin et al. 1995; Oomens et al. 2001b), and the observed profiles of some interstellar IR emission features indicate that these effects are important for interstellar emission spectra (Verstraete et al. 2001; Pech et al. 2002). Only a few systems have been studied experimentally, and for a detailed comparison between models and the observations, further laboratory studies are imperative.

In this paper, we present a critical comparison of IR spectra of specific PAHs obtained with different techniques and of theoretical quantum chemical calculations in order to elucidate the advantages and disadvantages of these techniques. The emphasis is on the infrared characteristics of PAH cations, which are thought to dominate the emission in the critically important 6–9 μm, CC stretching and CH bending regions. These results provide essential input to astronomers for their models of the infrared emission spectra of interstellar or circumstellar sources. In addition, we also present, for the first time, the results of an experimental study of the anharmonic parameters of the vibrational modes of the naphthalene and coronene cations and compare these with a previous study of the neutrals of these species.

This paper is organized as follows: In § 2, we present an overview of experimental techniques, focusing on IR multiple-photon dissociation of trapped ions. The infrared spectra of individual PAH cations are compared in § 3, while general trends are discussed in § 4. In § 5, we model laboratory and interstellar infrared spectra, including the effects of anharmonic interactions. The astrophysical implications are assessed in § 6. Our results are summarized in § 7.

2. OVERVIEW OF EXPERIMENTAL TECHNIQUES

Different experimental techniques have proven to be useful to study the infrared spectroscopy of ionic PAHs. Obviously, standard gas-phase infrared techniques, such as direct absorption or Fourier transform spectroscopy, are not applicable because of the very low number density that one can obtain as a consequence of space charge limitations. We give here a brief overview of techniques that are successfully applied in infrared spectroscopy of ionic PAHs: matrix isolation spectroscopy, van der Waals cluster dissociation spectroscopy, single-photon infrared emission spectroscopy, and multiple-photon dissociation spectroscopy, the latter being discussed to a somewhat larger extent.

We note here that besides these techniques, information on the vibrational structure of the electronic ground state of cationic PAHs has also been obtained by applying threshold ionization techniques. The most widely used methods nowadays are the zero kinetic energy (ZEKE; Müller-Dethlefs & Schlag 1991) and mass-analyzed threshold ionization (MATI; Zhu & Johnson 1991) spectroscopy. Both methods have been successfully applied to the study of aromatic molecules; as an example, we mention the ZEKE spectra of pyrazine (Hillenbrand, Zhu, & Johnson 1991) and the MATI spectra of different fluorene-Ar_n clusters (Zhang et al. 1997). However, it is important to note that selection rules are fundamentally different using these techniques, and moreover, intensities are strongly affected by Franck-Condon overlap, so that they are of limited use in obtaining true infrared spectral information on these ionic PAHs. Another interesting method relies on the knowledge that the IR spectrum of a molecule in a high Rydberg state resembles that of the corresponding cation very closely. Using UV lasers, the molecule is excited to a high Rydberg state and subsequent IR excitation of vibrational modes in the ionic core causes the total internal energy to exceed the ionization potential, which eventually leads to autoionization of the Rydberg neutral (Fujii et al. 1997, 1999; Gerhards et al. 1998). These ions can then be detected in a time-of-flight (TOF) mass spectrometer. However, the ionization probability appears to be vibrational mode–dependent, yielding less reliable IR intensities. Moreover, little or no work on pure PAH^+ compounds has been reported thus far.

2.1. *Matrix Isolation Spectroscopy* (*MIS*)

Infrared spectra of cationic PAHs isolated in rare gas matrices have mainly been obtained by the groups of Vala in Gainesville, Florida (Szczepanski et al. 1992, 1993, 2002; Szczepanski & Vala 1993; Vala et al. 1994) and Allamandola at NASA Ames (Hudgins, Sandford, & Allamandola 1994; Hudgins & Allamandola 1995a, 1995b, 1997; Hudgins et al. 2000). At present, matrix-isolated data constitute the main body of experimental infrared spectroscopic information on cationic PAHs.

In a vacuum chamber, vaporized PAHs are embedded in a cryogenic matrix (usually Ar or Ne). The embedded neutral PAHs are irradiated with a bright UV lamp to induce ionization. A (Fourier transform) infrared spectrometer is then used to record a spectrum of the matrix-isolated ionic PAHs. Since only a small fraction of the PAHs become ionized, the spectrum also contains many lines originating from neutral PAHs, and moreover, bands due to anions or fragments may be present. In order to determine whether a band is due to the cationic PAH, various correlation measurements are usually necessary. Alternatively, ions can be created ex situ and mass-selectively deposited in the matrix to overcome some of the mentioned problems. This approach has only been applied to a limited number of species thus far.

Since the rotation of matrix-isolated species is quenched and the temperature is low, narrow absorption bands are usually observed. Depending on the resolution of the spectrometer, line widths on the order of 1 cm^{-1} are commonly

obtained. There has been substantial debate as to the influence of the matrix on the spectrum. Although infrared band positions appear to be little affected by the matrix, Joblin et al. (1994) reported up to fivefold changes in the relative intensities of MIS spectra of neutral PAHs relative to their gas-phase spectra.

2.2. *Dissociation Spectroscopy of van der Waals Clusters* (*VDW*)

The VDW method relies on the knowledge that attaching a loosely bound noble gas atom to a gas-phase PAH hardly influences its infrared spectrum. The binding energy of the attached "messenger" atom is so low, typically around 300 cm^{-1} for Ar, that absorption of an infrared photon will detach it from the PAH chromophore, thus serving as an absorption signal in a mass spectrometer (Okumura et al. 1986). The PAH noble gas van der Waals clusters are formed in the supersonic expansion of a molecular beam. Applying a resonance-enhanced ionization scheme to just barely above the ionization potential of the cluster yields an ionic PAH noble gas van der Waals cluster. This ionic cluster can then be spectroscopically interrogated with a tunable infrared laser, where the bare PAH ion is produced whenever the laser wavelength is in resonance with a transition in the PAH cluster ion.

The technique has been successfully applied in the CH stretching region around 3 μm using parametric oscillator (Dopfer, Olkhov, & Maier 1999; Dopfer, Roth, & Maier 2002) and difference frequency sources (Fujii et al. 2000) and in the 5–25 μm fingerprint infrared region using a free electron laser (FEL; Satink et al. 1999; Piest et al. 1999, 2001; Bakker et al. 2002).

In terms of band shifts, the perturbation of the rare gas atom on the spectrum of the chromophore was indeed found to be very small, typically 1 cm^{-1} (Fujii et al. 1997; Bakker et al. 2002), which is usually within the accuracy of the experiment. More subtle effects, such as the appearance of van der Waals sidebands and symmetry breaking effects, were recognized in the VDW spectra of cationic benzene (Bakker et al. 2002). Observed line widths are typically on the order of 5 cm^{-1}, determined mainly by the bandwidth of the (pulsed) laser systems used and/or the rotational envelope of the jet-cooled species. Even for a relatively small molecular system (aniline) and excitation to just slightly above the cluster dissociation limit, predissociation lifetimes were recently measured to range from a few tens to a few hundreds of nanoseconds (Satink et al. 2002). Since the time delay between the infrared pulse and extraction into the TOF mass spectrometer is typically (at least) several microseconds, these predissociation lifetimes are not expected to affect relative intensities in the spectrum.

2.3. *Infrared Emission Spectroscopy* (*IRE*)

In order to verify whether (ionized) PAHs are the true carriers of the observed unidentified infrared bands (UIRs), one would ideally like to obtain laboratory infrared PAH spectra in emission, because this is likely closest to interstellar spectra. The infrared radiation that is emitted by a hot sample of PAHs can indeed be dispersed by an infrared spectrometer so that true emission spectra are obtained. Thus, infrared emission spectra of various neutral PAHs have been reported mainly in the 3 μm CH stretching region, where high internal energies are achieved via either UV excitation (Cherchneff & Barker 1989; Brenner & Barker 1992; Shan, Suto, & Lee 1991)—note the correspondence with interstellar PAHs!—or heating in an oven (Kurtz 1992).

However, in the wavelength region longward of $\approx$5 μm, this method becomes very challenging because of the blackbody radiation of the laboratory instruments at room temperature. Therefore, one has to either correct for the blackbody contribution (Kurtz 1992) or use a cryogenically cooled spectrometer. This latter method has been successfully applied by the group of Saykally in the 5–20 μm spectral range, and emission spectra of several neutral PAHs (Schlemmer et al. 1994; Cook et al. 1998) were reported as well as that of cationic pyrene (Kim, Wagner, & Saykally 2001).

2.4. *Multiple-Photon Dissociation of Trapped Ions* (*MPD*)

IR MPD of ionic species stored in an ion trap was first shown to be possible using powerful line-tunable CO_2 lasers (Shin & Beauchamp 1990; Peiris et al. 1993). A recent overview of (dissociation) spectroscopy of trapped ions is given by Dunbar (2000). The application of a widely tunable FEL allows us to record infrared spectra of various cationic PAHs over the fingerprint infrared range between 500 and 1800 cm^{-1}.

The experimental apparatus as shown in Figure 1 was previously described by Oomens et al. (2000). The solid PAH sample is placed in an oven, and the vapor effuses into a vacuum chamber. In the center of a quadrupole ion trap (Paul 1990) (R. M. Jordan Co.), the vapor-phase molecules are photoionized with the 193 nm radiation of a small ArF excimer laser. The ionized photoproducts, i.e., the parent ion and ionic fragments, are instantaneously trapped. The contents of the trap can be analyzed in a TOF mass spectrometer by extracting the ions into the 60 cm TOF tube. This is achieved by turning off the radio frequency (RF) trapping potential and applying a 200 V dip to the end cap closest to the detector. Synchronously with this extraction pulse, a digital 10 bit oscilloscope (Yokogawa DL4200) is triggered, capturing the transient from the microchannel plate (MCP) detector. The transient is averaged and then read into a PC.

A rich fragmentation pattern is usually induced by the ArF laser, as is shown for phenanthrene by the upper trace in Figure 2. Being the heaviest species present, the parent PAH is easily isolated using the axial ejection properties of the ion trap (March & Londry 1995). Increasing the amplitude of the RF voltage such that the Mathieu q_z parameter becomes greater than 0.91 for all fragment ions ejects all ions smaller than the parent PAH cation from the trap. In these experiments, we found that a 2 ms duration increase of V_{RF} efficiently removes fragment ions from the trap so that a clean isolated sample of the parent ion is obtained. This is shown by the middle trace in Figure 2. After this isolation step, the RF amplitude is reset to some intermediate value so that fragments produced subsequently by IR MPD remain stored in the ion trap and can be detected background-free, as described below.

The isolated ion cloud is now irradiated with the intense and narrowband infrared radiation of the Free Electron Laser for Infrared Experiments (FELIX; Oepts, van der Meer, & van Amersfoort 1995), which is focused in the cen-

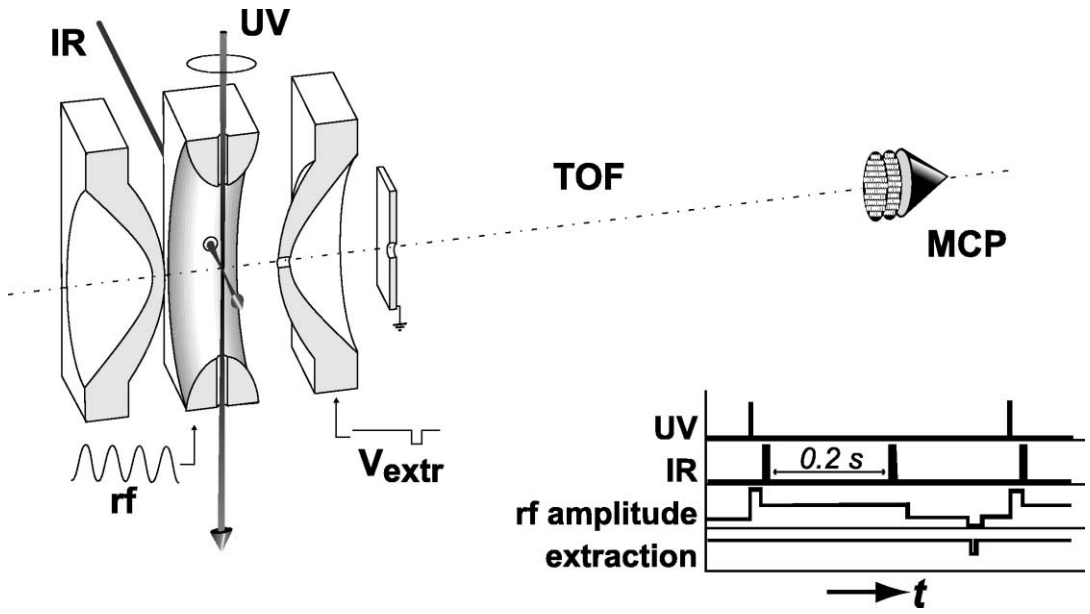

FIG. 1.—Impression of the experimental setup used to obtain infrared MPD spectra of cationic PAHs, showing a cut through the ion trap, the TOF mass spectrometer with MCP detector, and the UV and IR laser beams for ionization and dissociation, respectively. The inset shows a typical pulse sequence for UV and IR laser pulses, trapping RF amplitude, and extraction pulse.

ter of the ion trap, as sketched in Figure 1. FELIX typically produces 50 mJ macropulses of 5 μs duration at a 5 Hz repetition rate. Each macropulse consists of a train of adjustable duration (0.1–10 ps) micropulses separated by 1 ns. The bandwidth is determined by the micropulse duration and was typically 0.6% FWHM of the central wavelength in this experiment. If the wavelength of FELIX is in resonance with an allowed infrared transition of the PAH cation, multiple-photon absorption can occur by virtue of the high laser fluence.

The lower trace in Figure 2 represents the mass spectrum of the isolated phenanthrene cation after irradiation with two macropulses of FELIX at $\lambda = 8.0$ μm. Multiple-photon infrared absorption leads to the detachment of an acetylenic

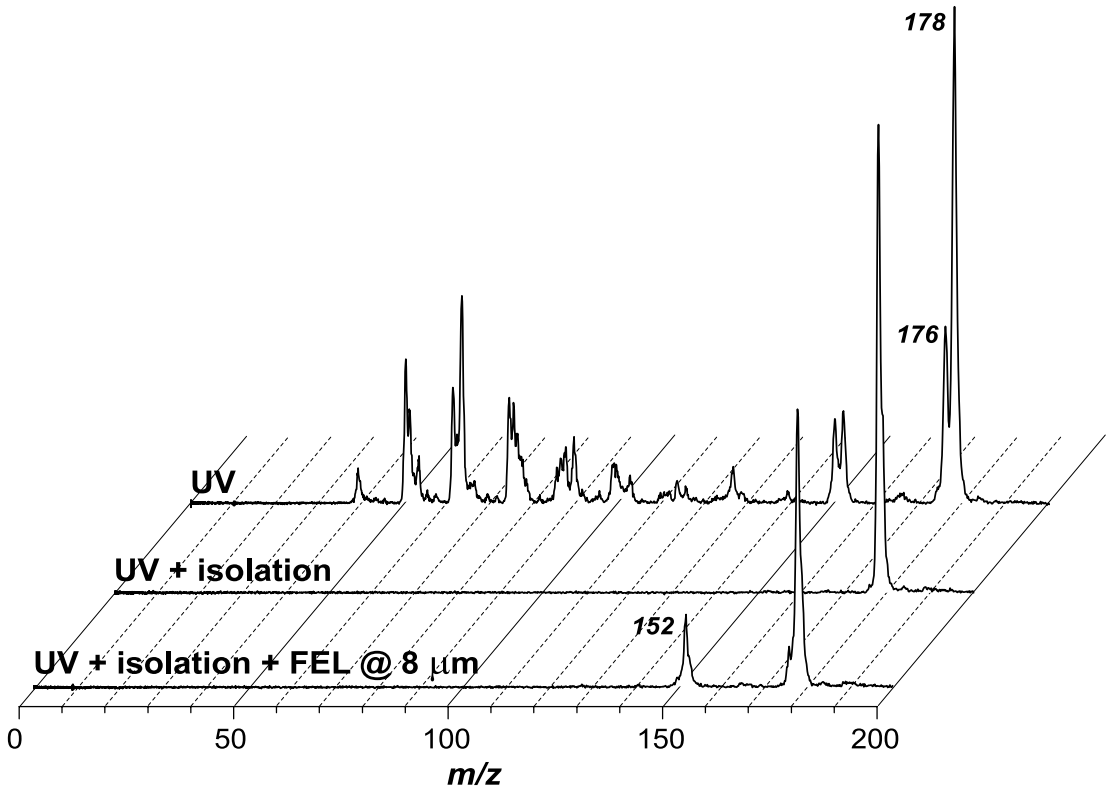

FIG. 2.—Mass spectra of cationic phenanthrene in the experimental sequence used in the IR MPD technique

unit forming the $C_{12}H_8^+$ fragment ion at $m/z = 152$. From the values for the ionization potential of the parent molecule and the appearance energies for the ionic fragments, dissociation thresholds for the fragmentation channels can be estimated to be on the order of 6–8 eV, which corresponds to more than 50 photons at $\lambda = 10\ \mu$m. A more detailed discussion on the multiple-photon absorption process involved in these experiments can be found elsewhere (Oomens et al. 2000; Oomens, Meijer, & von Helden 2001a). To record the infrared spectrum of the parent ion, the intensity in the fragment channel is recorded while the wavelength of FELIX is scanned.

During the interaction with the infrared laser, the RF amplitude is kept at a fairly high value, which creates a better overlap between the ion cloud and the laser focus resulting in an enhanced fragmentation yield. However, such a high RF amplitude substantially deteriorates the resolution in the subsequently recorded mass spectrum. We therefore lowered the RF amplitude approximately 30 ms before the extraction pulse was triggered, as indicated in the timing sequence in Figure 1. An arbitrary waveform generator (Wavetek 39) was used to control the RF amplitude via the external input on the ion trap power supply (Jordan Co.). During extraction, the RF is automatically switched off by the power supply.

3. COMPARISON OF INDIVIDUAL PAH CATION SPECTRA

In this section, we compare spectra of ionic PAHs that were obtained via different experimental methods. Since each technique possesses its own characteristics in terms of line width, etc., we convoluted reported line positions and relative intensities with a 30 cm^{-1} FWHM Lorentzian line width. This facilitates a comparison of the spectra obtained with MPD, MIS, VDW, and IRE, as is shown in Figure 3. Moreover, all spectra are compared to density functional theory (DFT) calculations. Although DFT-calculated spectra for these species have been reported previously (Pauzat et al. 1992; DeFrees et al. 1993; Langhoff 1996; Bauschlicher et al. 1999; Oomens et al. 2001a), we recalculated all spectra using the B3LYP method and the D95(d, p) basis set as implemented in Gaussian 98 (Frisch et al. 1998) to be able to make a more consistent comparison. No frequency scaling has been applied to the calculated spectra. Table 1 gives a complete overview of all available experimental data, including species that were investigated with only one technique. Below we briefly discuss species for which more than one experimental spectrum is available (see Fig. 3).

Naphthalene.—The VDW cluster dissociation spectrum of Piest et al. (1999) appears to give the most detailed results. In both frequencies and relative intensities, the correspondence with theory is very good, except for the band near 1030 cm^{-1}, which appears to be too weak in the calculation. However, this low intensity appears to be in agreement with experimental results from both the MIS and MPD spectra. The MIS spectrum fails to reproduce some of the weaker lines in the spectrum, whereas in the MPD spectrum, the band in the 1500 cm^{-1} range is very broad, perhaps suggesting a doublet.

Phenanthrene.—The detailed VDW cluster dissociation spectrum of Piest et al. (2001) recently showed that DFT has great difficulties calculating the spectrum of cationic phenanthrene, in particular in the region between 900 and 1300 cm^{-1}. This was verified by our MPD spectrum (Oomens et al. 2000), and based on these findings, the assignments of the previously published MIS spectrum (Hudgins & Allamandola 1995a) were updated (Piest et al. 2001). It was suggested that a low-lying electronic state perturbs the vibrational structure of the ground electronic state, leading to large deviations from DFT theory.

Anthracene.—MIS and MPD spectra are available for the anthracene cation (Szczepanski et al. 1993; Hudgins & Allamandola 1995b; Oomens et al. 2000). Both spectra show significant deviations from DFT calculations, in particular in the in-plane CH bending region around 1400 cm^{-1}, where the strongest bands are located. Of the three b_{2u} symmetry bands calculated at 1210, 1395, and 1445 cm^{-1}, the one at 1395 cm^{-1} is particularly strongly redshifted in both experimental spectra. Since all three modes have b_{2u} symmetry (D_{2h} point group), the bands are possibly subject to anharmonic interaction, particularly so since all three modes have strongly delocalized in-plane CH bending as well as CC stretching character, as is shown in Figure 4. This was previously suggested by Szczepanski et al. (1993). Since the 1395 and 1445 cm^{-1} modes are closest in energy, they are the most likely to show the effects of such an interaction, which would be to increase the spacing between the two modes. An interaction matrix element $W \approx 30$ cm^{-1} can be shown to increase the theoretical spacing of 50 cm^{-1} to the value of 77 cm^{-1}, as observed in the MIS spectrum. The spacing is even slightly bigger in the MPD spectrum, likely because of (nonuniform) redshifting as a consequence of additional interactions with background states.

In addition, there appear to be some discrepancies in the weak bands observed in the 800–1100 cm^{-1} range, as well as in the blue part of the spectrum between 1500 and 1700 cm^{-1}.

Pyrene.—Besides MIS (Szczepanski & Vala 1993; Hudgins & Allamandola 1995a) and MPD (Oomens et al. 2000) spectra, the IRE spectrum of cationic pyrene has been reported recently by the group of Saykally (Kim et al. 2001). All spectra compare reasonably well, except in the range 1200–1500 cm^{-1}, where the IRE spectrum appears to deviate substantially from MIS and MPD data. In particular, the strong band that is observed between 1350 and 1400 cm^{-1} in the MIS and MPD spectra is reported below 1300 cm^{-1} in the IRE spectrum. Moreover, intensities for the bands around 1350 cm^{-1} relative to the 1550 cm^{-1} band vary severely between all experimental spectra. The weak feature(s) near 950 cm^{-1} were not observed in the IRE spectrum.

Coronene.—The MIS spectra of coronene (Szczepanski & Vala 1993; Hudgins & Allamandola 1995a) report an anomalous intensity of the CH out-of-plane bending mode relative to the CH in-plane bending and CC stretching bands at shorter wavelengths. In the recently reported MPD spectrum (Oomens et al. 2001b), however, no anomalous intensity ratio is found. The ratio observed is as is generally found for cationic PAHs and appears to be in good agreement with DFT calculations. It may be noted that the coronene cation is subject to Jahn-Teller distortion, and, therefore, the calculation was carried out in the D_{2h} symmetry group.

For a number of neutral PAHs, it was experimentally shown by Joblin et al. (1994) that matrix isolation may severely affect the relative intensities of the different bands with respect to those in a gas-phase spectrum. In general,

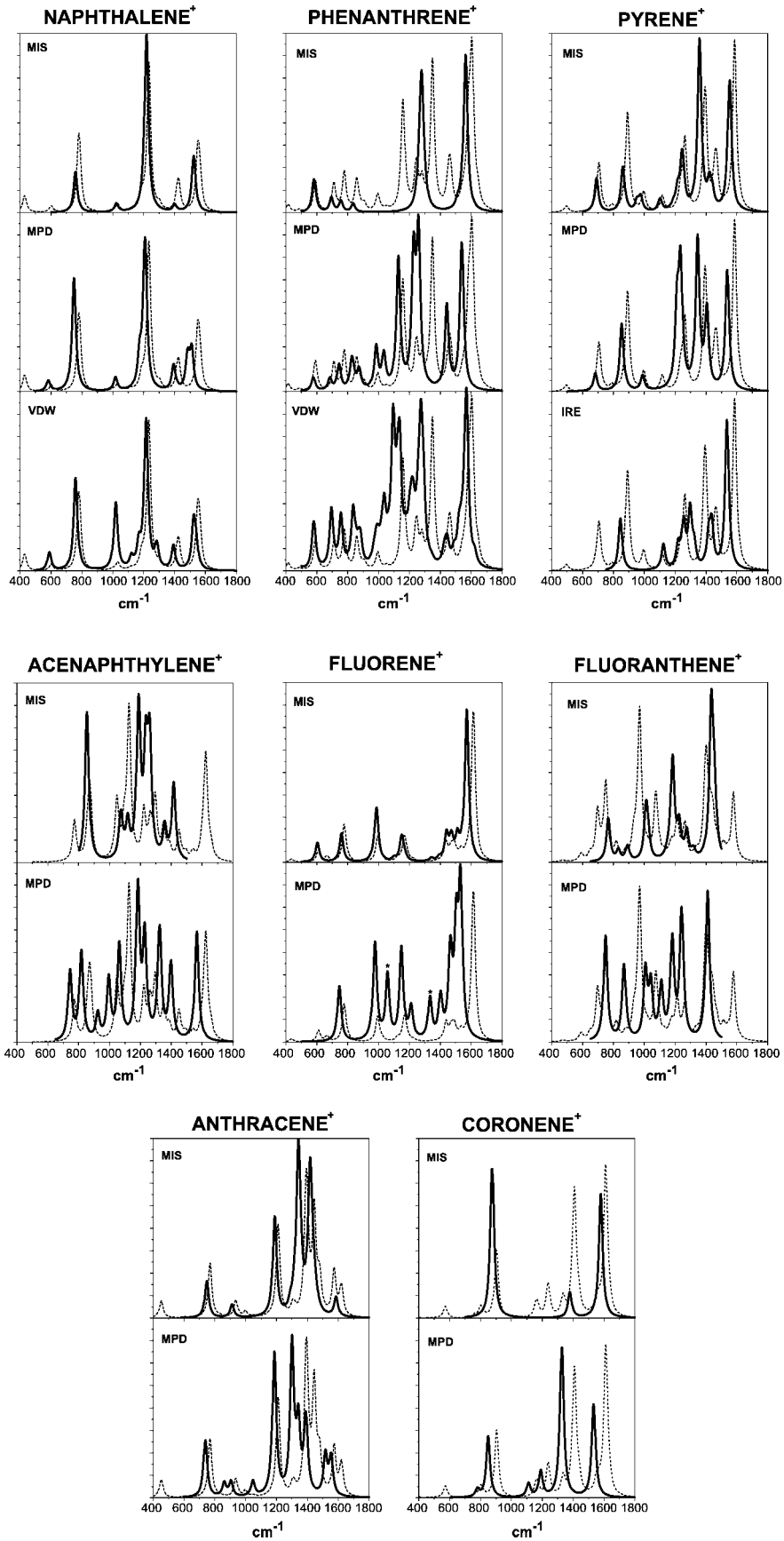

FIG. 3.—Infrared spectra of cationic PAHs that were studied using different experimental techniques. The spectra are generated from reported experimental frequencies and intensities, convoluted with a 30 cm^{-1} FWHM Lorentzian line width. The dotted lines represent DFT calculations [B3LYP functional, D95(*d*, *p*) basis, no frequency scaling].

TABLE 1
OVERVIEW OF EXPERIMENTAL PAH^+ SPECTRA

PAH^+	Method	Range (cm^{-1})	References
C_6H_6: benzene	VDW[a]	450–1500	Satink et al. 1999
	VDW	2850–3150	Dopfer et al. 1999
	VDW[a]	300–3200	Bakker et al. 2002
C_9H_{10}: indane	MPD	600–1700	Oomens et al. 2001a
$C_{10}H_8$: naphthalene	MIS	800–1600	Szczepanski et al. 1992
	MIS[a]	700–1600	Hudgins et al. 1994
	VDW	400–1650	Piest et al. 1999
	MPD	500–1700	Oomens et al. 2000
$C_{12}H_8$: acenaphthylene	MIS	900–1600	Banisaukas et al. 2003
	MPD	650–1700	Banisaukas et al. 2003
$C_{12}H_{10}$: acenaphthene	MPD	700–1600	Oomens et al. 2001a
$C_{13}H_{10}$: fluorene	MPD	550–1800	Oomens et al. 2001a
	MIS	500–1600	Szczepanski et al. 2002
$C_{14}H_{10}$: phenanthrene	MIS[a]	500–1600	Hudgins & Allamandola 1995a
	MPD	500–1800	Oomens et al. 2000
	VDW[a]	400–1700	Piest et al. 2001
$C_{14}H_{10}$: anthracene	MIS	400–1600	Szczepanski et al. 1993
	MIS	700–1600	Hudgins & Allamandola 1995b
	MPD	500–1650	Oomens et al. 2000
$C_{16}H_{10}$: pyrene	MIS[a]	650–1600	Vala et al. 1994
	MIS[a]	500–1600	Hudgins & Allamandola 1995a
	MPD	500–1600	Oomens et al. 2000
	IRE	800–4000	Kim et al. 2001
$C_{16}H_{10}$: fluoranthene	MIS	700–1500	Hudgins et al. 2000
	MPD	650–1500	Oomens et al. 2001a
$C_{18}H_{12}$: tetracene	MIS	900–1650	Hudgins & Allamandola 1995b
$C_{18}H_{12}$: chrysene	MIS	600–1600	Hudgins & Allamandola 1997
$C_{18}H_{12}$: 1,2–benzanthracene	MIS	900–1600	Hudgins & Allamandola 1997
$C_{18}H_{12}$: triphenylene	MPD	550–1650	Oomens et al. to be published
$C_{20}H_{12}$: perylene	MIS	700–1600	Szczepanski & Vala 1993
$C_{20}H_{12}$: benzo[e]pyrene	MIS	500–1600	Hudgins & Allamandola 1995a
$C_{20}H_{12}$: benzo[a]fluoranthene	MIS	600–1600	Hudgins et al. 2000
$C_{20}H_{12}$: benzo[b]fluoranthene	MIS	550–1600	Hudgins et al. 2000
$C_{20}H_{12}$: benzo[j]fluoranthene	MIS	700–1600	Hudgins et al. 2000
$C_{20}H_{12}$: benzo[k]fluoranthene	MIS	650–1600	Hudgins et al. 2000
$C_{22}H_{12}$: benzo[ghi]perylene	MIS	500–1600	Hudgins & Allamandola 1995a
$C_{22}H_{14}$: pentacene	MIS	700–1600	Hudgins & Allamandola 1995b
$C_{24}H_{12}$: coronene	MIS	800–1400	Szczepanski & Vala 1993
	MIS	500–1600	Hudgins & Allamandola 1995a
	MPD	650–1650	Oomens et al. 2001b
$C_{42}H_{18}$: hexabenzocoronene–A	MIS	600–1700	Bakes et al. 2001b
$C_{48}H_{20}$: dicoronylene	MIS	800–1700	Bakes et al. 2001b

[a] Perdeuterated species reported as well.

CH out-of-plane modes were found to appear weaker as a result of matrix isolation. However, in the reported MIS spectra of cationic coronene, this trend is opposite, so that the discrepancy between MIS and MPD data remains puzzling.

Fluorene.—The MIS data for the fluorene cation (Szczepanski et al. 2002a) are very close to the DFT result. The MPD spectrum shows additional features at 1058 and 1334 cm^{-1} (indicated with an asterisk in Fig. 3), which were, however, shown to be due the dehydrogenated fragment $C_{13}H_9^+$ (Oomens et al. 2001a). In addition, the appearance of extra bands as a shoulder in the long-wavelength flank of the strongest band at 1532 cm^{-1} is likely due to strong anharmonicity of this mode in combination with weaker fundamental bands in this region. Bearing these considerations in mind, there is good correspondence between MIS, MPD, and DFT spectra of the fluorene cation.

Fluoranthene.—Bauschlicher et al. (1999) extensively discussed computational problems for the fluoranthene cation. In particular, the commonly used B3LYP functional causes errors, and, therefore, the BP86 functional (Perdew 1986; Becke 1988) was used; however, the calculated spectrum is still in severe disagreement with observations of MIS as well as of MPD. The low overall absorption strength of this species (Hudgins et al. 2000) gives only moderate experimental results. Nonetheless, the two experimental spectra show reasonable agreement, although the MPD spectrum appears to yield more intensity in the 1000–1250 cm^{-1} region, where, in fact, heavy spectral congestion occurs. The out-of-plane CH bending mode observed at 869 cm^{-1}

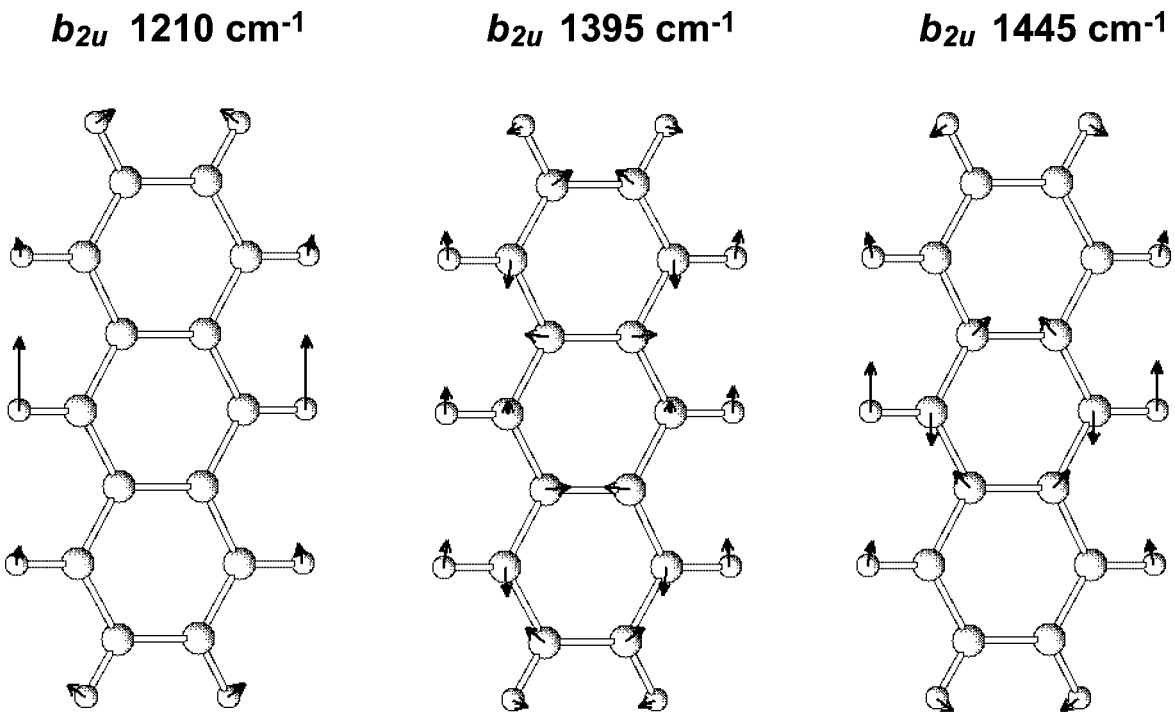

FIG. 4.—Atom displacements of three high-intensity vibrational modes of the anthracene cation. All modes have b_{2u} symmetry and strongly delocalized in-plane CH bending and CC stretching character. In particular, the closely spaced modes calculated at 1395 and 1445 cm^{-1} may well be subject to anharmonic interaction.

in the MPD spectrum appears only very weakly in the MIS spectrum.

Acenaphthylene.—MIS and MPD spectra of acenaphthylene were recorded very recently (Banisaukas et al. 2003). Acenaphthylene is expected to be extremely stable under astrophysical conditions (Ekern et al. 1998; Jochims, Baumgärtel, & Leach 1999) and therefore forms a particularly interesting candidate to be studied experimentally. On the other hand, this feature of the acenaphthylene cation also makes MPD difficult since only very weak H_2 loss is observed under resonant infrared irradiation. Most of the features observed in the MIS spectrum can also be recognized in the MPD spectrum, where the lines appear to be extraordinarily broad, leading to high spectral congestion. On the other hand, in the MIS spectrum, the spectral regions around 750, 1000, and 1550 cm^{-1} were inaccessible because of overlapping bands of contaminants in the matrix. Taking these experimental limitations into account, the two spectra agree fairly well. However, particularly in the in-plane CH bending region, they show considerable deviations from the DFT spectrum. In this spectral range, where severe congestion occurs, the strongest bands in the experimental spectra are blueshifted with respect to those in the theoretical spectrum. It may be noted that a calculation using the BP86 functional yields significant differences compared to the B3LYP spectrum, especially in the in-plane CH bending range (Banisaukas et al. 2003), possibly pointing to a flaw in the theoretical spectrum.

Other.—Many other species have been studied with only one of the mentioned experimental techniques, and, therefore, they can only be compared to theoretical spectra. Some interesting species are mentioned below.

The spectrum of cationic benzene (Satink et al. 1999; Bakker et al. 2002) shows severe discrepancies with respect to the DFT calculation, which was shown to be due to a combination of Jahn-Teller distortion (Jahn & Teller 1937) and strong Fermi interaction. Curiously, no MIS spectra have to date been reported for this benchmark species.

The spectrum of the triphenylene cation (to be published) deviates substantially from the calculated spectrum of Langhoff (1996). Although the exact reason for this disagreement requires further analysis, we may note that the ion, being of D_{3h} symmetry, is subject to Jahn-Teller distortion. Moreover, in contrast to some other Jahn-Teller active species such as the benzene and coronene ions, the normal modes giving rise to Jahn-Teller interaction in ionic triphenylene are infrared-active (Keszthelyi et al. 2000).

Larger species (larger than 48 C atoms) have thus far exclusively been studied theoretically (Bauschlicher & Bakes 2000; Bauschlicher 2002).

4. GENERAL COMPARISON

We now discuss the general trends that arise from the comparison of the individual PAH ion spectra in the previous section.

1. *Band positions.*—In the long-wavelength region of the spectra where the CH out-of-plane bending modes are located, band positions are determined by the number of neighboring hydrogen molecules on an aromatic ring (Hudgins & Allamandola 1999b). All experimental spectra are in good agreement with this general rule.

On the blue end of the spectra, where the CC stretching modes are located,[6] it may be noted that the CC stretching mode falls at nearly the same position for all species investigated. In the MIS spectra, this band is located in a 50 cm^{-1} window around 1570 cm^{-1} and in the MPD spectra in a similar spectral window centered around 1530 cm^{-1}.

The situation is completely different for the in-plane CH bending mode(s) in the 1100–1500 cm^{-1} range. In both the MIS and the MPD spectra, the bands in this range show more scattering from molecule to molecule. This striking difference between the CC stretching and in-plane CH bending regions may have important implications relevant to the UIR spectrum, as will be discussed in § 6.

2. *MPD line widths.*—In the MPD spectra, the modes around 1200–1700 cm^{-1}, being CH in-plane bending and CC stretching modes, in general appear to be broader than bands in the longer wavelength range of the spectrum, particularly in the 500–800 cm^{-1} region, where the CH out-of-plane bending modes are located. In Figure 5, a comparison between these two spectral regions is shown for the MPD spectra of eight PAH cations. MIS experimental spectra have been represented by vertical lines. Although in some cases one could argue that the enhanced line width is due to a convolution over several unresolved bands, in the more sparse spectra of, e.g., naphthalene and coronene, line widths are clearly seen to be larger in the blue part of the spectrum.

This effect may be explained by assuming that these modes in general show larger anharmonicity, as was explicitly demonstrated for neutral and ionic coronene (Joblin et al. 1995; Oomens et al. 2001b). Unfortunately, hardly any experimental data are available on anharmonicity parameters of (ionic) PAHs. Moreover, standard DFT calculations apply a harmonic approximation, thereby neglecting anharmonic properties of the molecule so that hardly any information is available from theory. However, comparison of the available linear absorption data (MIS/VDW) with the multiple-photon absorption data (MPD) may provide an important clue to estimate the influence of anharmonicity on the different spectral regions, as is discussed below.

3. *Anharmonic redshifts.*—In Figure 3, one can clearly observe that the bands in the MPD spectra are consistently redshifted with respect to their counterparts in the MIS spectra. As mentioned, this is due to the influence of vibrational (cross-)anharmonicities in molecules at higher levels of excitation. Here we will attempt to quantify the effect by determining the differences in band centers of corresponding bands in the MIS and MPD spectra. An average band shift is then determined for each of the three major spectral regions, the out-of-plane CH bending range (500–1000 cm^{-1}), the in-plane CH bending range (1000–1450 cm^{-1}), and the CC stretching range (1450–1600 cm^{-1}). Table 2 lists the individual redshifts of bands for which the correspondence between MIS and MPD appeared to be reasonably secure, along with the resulting average shifts.

As shown in Table 2, the standard deviation of the average redshift in the in-plane CH bending region of the spectrum (26%) is larger than the deviations in the out-of-plane CH bending region (14%) and in the CC stretching region (13%). As mentioned in (1), the spectra are usually most complex in the in-plane CH bending region, and, therefore, it may be more difficult to find the correct correspondences between MIS and MPD data here. Moreover, in this region, heavy spectral congestion occurs particularly in the MPD spectra. However, the higher degree of scattering in the values for the redshifts may also have a molecular nature, just as the band positions appear to show more scattering in this region.

It is also seen that the absolute anharmonic redshift is significantly larger in the CC stretching region than in the out-of-plane CH bending region. Note, by the way, that since there is roughly a factor of 2 in the frequency range, the relative shift is about the same. This observation could well explain the differences in line widths in the two spectral regions as being indeed due to larger anharmonic interactions in the shorter wavelength range.

4. *Five-membered ring species.*—In contrast to regular PAH ions, several of the PAHs incorporating a five-membered ring show a fairly strong absorption near 1000 cm^{-1} (Hudgins et al. 2000; Bauschlicher et al. 1999; Oomens et al. 2001a), particularly fluorene, fluoranthene, and possibly acenaphthylene (for the latter, MIS, MPD, and calculated data remain inconclusive as to the presence of this

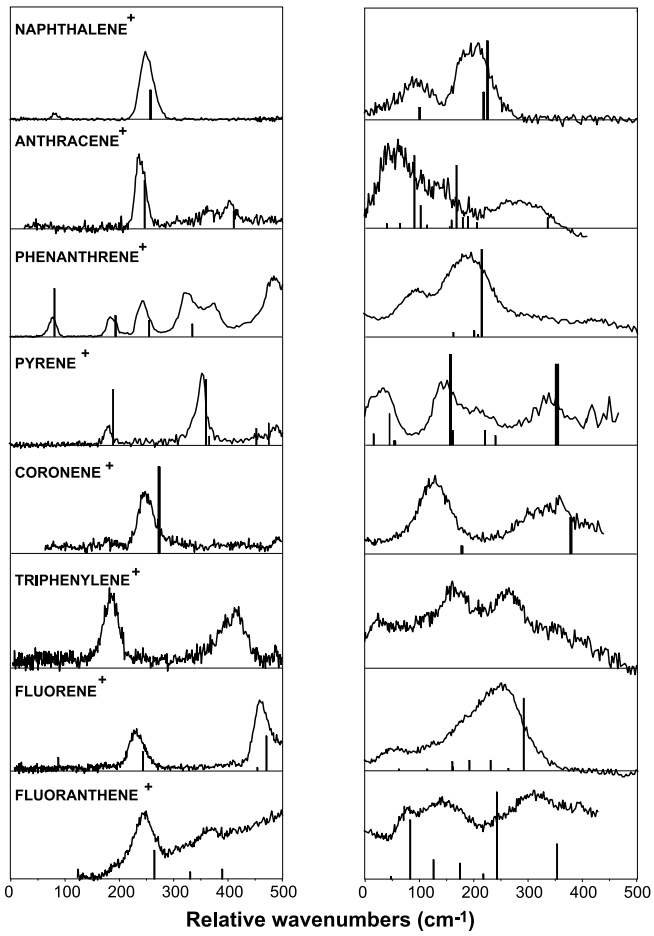

FIG. 5.—Comparison of line widths in the MPD spectra. The left-hand column shows spectra in the CH out-of-plane bending region roughly between 500 and 1000 cm^{-1}, and the right-hand column shows the spectra in the CC-stretch/CH in-plane bending region roughly between 1200 and 1700 cm^{-1}. Vertical scales are flexible. The stick spectra represent matrix data.

[6] Calculations show that, in general, vibrations in the 1200–1700 cm^{-1} range have both CC stretching and in-plane CH bending character, mixed to various extents. A good example is shown in Fig. 4 for the anthracene cation. However, in accordance with common astrophysical practice, we shall designate the 1100–1500 cm^{-1} range as the CH in-plane bending region and the 1500–1700 cm^{-1} range as the CC stretching region.

TABLE 2
MPD-MIS Band Position Differences

Range	Nph: $C_{10}H_8^+$	Fle: $C_{13}H_{10}^+$	Phn: $C_{14}H_{10}^+$	Ant: $C_{14}H_{10}^+$	Pyr: $C_{16}H_{10}^+$	Fla: $C_{16}H_{10}^+$	Cor: $C_{24}H_{12}^+$	Average[a]
500–1000.....	−10	−14	−4	−9	−18	−8	−26	−11.3 (1.6)
			−10	−7		−7		
			−12					
			−10					
1000–1450.....	−6	−10	−50	−1		−4	−52	−17.6 (4.5)
	−10	−1	−24	−39		−10		
	−7			−11		−12		
				−27				
1450–1650.....	−34	−40	−25	−32	−24	−15	−36	−27.6 (3.6)
	−15							

Note.—All values are in units of in cm^{-1}. Nph=naphthalene; Fle=fluorene; Phn=phenanthrene; Ant=anthracene; Fla=fluoranthene; Pyr=pyrene; Cor=coronene.
[a] Standard deviation in parentheses.

band). The astrophysical significance of this band is discussed in § 6.

5. *Intramolecular interactions*.—Low-lying electronic states may severely perturb the vibrational structure of the ground electronic state of the ion, leading to difficulties in the DFT-calculated spectrum. This was suggested to be the case for the phenanthrene (Piest et al. 2001) and fluoranthene (Bauschlicher et al. 1999; Hudgins et al. 2000) cations, where severe disagreements between calculated and experimental spectra are found.

Also, in many other cases, calculated spectra have shown severe discrepancies with respect to experimental data. The experimental VDW spectrum of the benzene cation is in strong disagreement with DFT calculations because of a combination of Jahn-Teller distortion and strong Fermi interaction (Satink et al. 1999; Bakker et al. 2002). The MPD spectrum of the triphenylene cation (to be published) also deviates strongly from DFT calculations, which is possibly due to Jahn-Teller distortion as well. On the other hand, it may be noted here that the spectrum of cationic coronene, subject to Jahn-Teller distortion as well, is well reproduced by calculations where the symmetry is lowered from D_{6h} to D_{2h}. Strong anharmonic interaction was suggested to cause the substantial deviation of MPD and MIS spectra of cationic anthracene from the DFT calculation. Finally, the MIS and MPD spectra of the acenaphthylene cation exhibit unexplained deviations from theory as well.

As a general conclusion, one could say that DFT calculations give fairly accurate results if the molecule behaves "regularly." However, in the case of strong perturbations or interactions, the spectra may change drastically, and current DFT methods are not able to account for them. Analysis of available experimental data has shown that such perturbations may be caused by low-lying electronic states, Fermi or anharmonic interactions, and Jahn-Teller distortion. Summarizing, it appears that the presence of at least one of these perturbations in the spectrum of a random PAH is not unusual.

5. MODELING MULTIPLE-PHOTON EMISSION AND ABSORPTION

It was already mentioned that a true interstellar emission spectrum is different from a standard linear absorption spectrum. Several publications deal with this issue (Barker et al. 1987; Schutte et al. 1993; Cook & Saykally 1998; Bakes et al. 2001a; Pech et al. 2002) and give mathematical models on how to generate an emission spectrum based on linear absorption data (line positions and relative intensities). An important difference between emission and linear absorption spectra is caused by the anharmonicity of vibrational potentials, which causes, for instance, the $2\nu_x \rightarrow \nu_x$ emission to be redshifted with respect to the fundamental $\nu_x \rightarrow 0$ emission. In the CH stretching region, this anharmonicity may cause redshifts on the order of 50 cm^{-1} per vibrational quantum (Barker et al. 1987).

Besides anharmonicity, cross-anharmonicity between the different vibrational degrees of freedom in a molecule should be taken into account. Cross-anharmonicity generally causes a specific transition (in both absorption and emission) to be redshifted in a hot molecule with respect to the same transition in a cold molecule. This is due to the anharmonic interaction between the vibrational mode emitting (or absorbing) radiation (ν_x) with the populated background vibrations ($\Sigma\nu_i$) in a hot molecule. Because of the extremely fast intramolecular vibrational distribution (IVR) in typical PAHs, the sum over the background states is highly dynamic and results in nothing other than an average vibrational temperature of the molecule. Thus, redshifting due to cross-anharmonicity is usually modeled as a temperature-dependent frequency shift, which is characteristic for each normal mode. The temperature dependence is usually taken to be linear; however, for the PAH systems under study, no theoretical anharmonicity data are available and from experiments only for very few (neutral) PAHs (see, e.g., Joblin et al. 1995). In the following, we will model the IR emission in terms of a molecule's internal energy E rather than its vibrational temperature T via the relation

$$E(T) = \sum_{i=1}^{s} \frac{h\nu_i}{\exp(h\nu_i/kT) - 1} , \qquad (1)$$

where s represents the number of vibrational degrees of freedom ($3N - 6$) and ν_i is the frequency of the ith mode (in units of cm^{-1}).

Both MPD and IRE involve highly excited species and are therefore affected by anharmonic shifting. However, the two processes are fundamentally different in that in contrast

TABLE 3
PARAMETERS USED IN THE CALCULATION OF MPD AND IRE SPECTRA OF $C_{24}H_{12}^+$

Frequency (cm^{-1})	I ($\times 10^{-17}$cm)	a[a] (cm^{-1})	b[b] (cm^{-1})
551	0.491	−1.000	0.762
763	0.226	−1.000	0.762
784	0.540	−1.000	0.762
881	3.170	−0.241	0.200
1147	0.626	−1.000	0.762
1213	1.480	−1.457	0.219
1311	0.630	−1.000	0.762
1353	4.990	−0.441	0.233
1355	0.885	−1.000	0.762
1382	0.763	−1.000	0.762
1504	0.292	−1.000	0.762
1505	0.633	−1.000	0.762
1553	7.540	−0.902	0.200
3087	0.403	−1.510	1.860
3088	0.502	−1.510	1.860

NOTE.—Only bands with $I > 2 \times 10^{-18}$ are listed.
[a] Anharmonic shift per vibrational quantum.
[b] Anharmonic broadening per vibrational quantum.

to infrared emission, multiple-photon excitation is a monochromatic[7] process. In particular, a mode possessing a large anharmonicity will be difficult to excite using monochromatic radiation, whereas no limitations obstruct the emission process. To assess these differences quantitatively, computer simulations of both types of spectra were carried out for the coronene cation, using the same molecular parameters taken from Joblin et al. (1995) and Langhoff (1996). These parameters are listed in Table 3 for the strongest IR bands of the ion. The anharmonicity parameters a_i describing the shift per vibrational quantum and b_i representing the increase in line width per vibrational quantum were derived from the experimental data for neutral coronene (Joblin et al. 1995). The χ_i' and χ_i'' parameters of Joblin et al. (1995) for anharmonic shifting and broadening, respectively, are related to our a_i and b_i parameters through equation (1) as

$$a_i = \chi_i' h\nu_i \left[\frac{dE(T)}{dT}\right]^{-1}, \quad b_i = \chi_i'' h\nu_i \left[\frac{dE(T)}{dT}\right]^{-1}. \quad (2)$$

Note that equation (1) yields an approximately linear E-T dependence at high energy, which for the coronene ion results in a value of $dE/dT \approx 64$ cm^{-1} K^{-1}. For vibrational modes for which no χ' and χ'' values are available, average values of $a = -1.000$ cm^{-1} and $b = 0.762$ cm^{-1} were assumed.

5.1. *IRE Model*

The IRE spectra are simulated using a model similar to those reported previously (Barker et al. 1987; Schutte et al. 1993; Cook & Saykally 1998; Bakes et al. 2001a); however, it includes the effects of anharmonic shifting and broadening of vibrational bands similar to a recently reported model by Pech et al. (2002). The coronene cation is assumed to be excited by a UV quantum in the range of $\hbar\omega_{UV} = 6$–12 eV, which is converted completely into to vibrational energy of the ground electronic state. The subsequent emission of IR quanta leads to vibrational cooling of the ion. In agreement with typical interstellar conditions, we suppose that radiative cooling is complete (in a few seconds) before the next UV quantum is absorbed.

Because of the emission cascade, the population distribution of the ensemble over the vibrational levels is determined by the radiative decay rates of the individual vibrational levels. The population of energy levels $E < \hbar\omega_{UV}$ was taken to be $p(E) = C/k(E)$, where $k(E)$ is the total rate of radiative decay at an energy E and C is a factor determined by the number density of the ions and the intensity of the UV radiation field. The radiative decay rate is calculated from the individual decay rates per vibrational mode i and per quantum v:

$$k_{i,v}(E) = A_{i,v} \frac{\rho^*(E - vh\nu_i)}{\rho(E)}, \quad (3)$$

where $A_{i,v}$ is the Einstein coefficient for spontaneous emission of the $v\nu_i \rightarrow (v-1)\nu_i$ transition, $\rho(E)$ is the density of states at energy E, and $\rho^*(E - vh\nu_i)$ is the density of states when the ith vibrational mode is excluded. Summation over all quanta v and subsequently over all modes i yields the total emission rate

$$k(E) = \sum_i k_i(E) = 8\pi c \sum_i \nu_i^2 A_i(E), \quad (4)$$

where $k_i(E)$ is the radiative decay rate of the ith vibrational mode in all quanta and $A_i(E) = \int_{\nu\sim\nu_i} \sigma(\nu, E) d\nu$ is the integral absorption cross section of ith vibrational mode at an energy E, $\sigma(\nu, E)$ being the absorption cross section. The dependence of $A_i(E)$ on E was calculated assuming infinitely fast energy redistribution among the vibrational modes of the ion (for details, see van Heijnsbergen et al. 2000).

The spectral form factor for the emitted quantum of the ith mode was assumed to be Lorentzian:

$$f_i(\nu) = \frac{1}{\pi} \frac{\Gamma_i(E)}{[\nu - \nu_i(E)]^2 + \Gamma_i(E)^2}, \quad (5)$$

where $\Gamma_i(E)$ is the bandwidth and $\nu_i(E)$ is the band center of the emitted radiation, both depending on the energy E of the radiatively decaying ion. The band center $\nu_i(E)$ is shifted from the fundamental frequency of the ith mode due to vibrational anharmonicity, commonly to longer wavelengths. The bandwidth $\Gamma_i(E)$ increases with vibrational energy because of the subpicosecond IVR processes, and for typical interstellar PAHs a Lorentzian width of 30 cm^{-1} was estimated at excitation energies $E \sim 10$ eV (Allamandola, Hudgins, & Sandford 1989). As in the MPD calculations (von Helden et al. 1999; van Heijnsbergen et al. 2000; Oomens et al. 2001b), we assumed the dependencies of ν_i and Γ_i on energy to be linear and used the experimental data reported for neutral coronene (Joblin et al. 1995).

Finally, the spectral dependence of the emitted radiation was obtained using

$$I(\nu) \sim \int \left[\sum_i f_i(\nu)\nu_i^2 A_i(E)\right] \rho(E)/k(E)\, dE, \quad (6)$$

where the density of vibrational states $\rho(E)$ was calculated using the Beyer-Swinehart algorithm (Stein & Rabinovitch

[7] The bandwidth of the infrared laser is 4 cm^{-1} in the calculation.

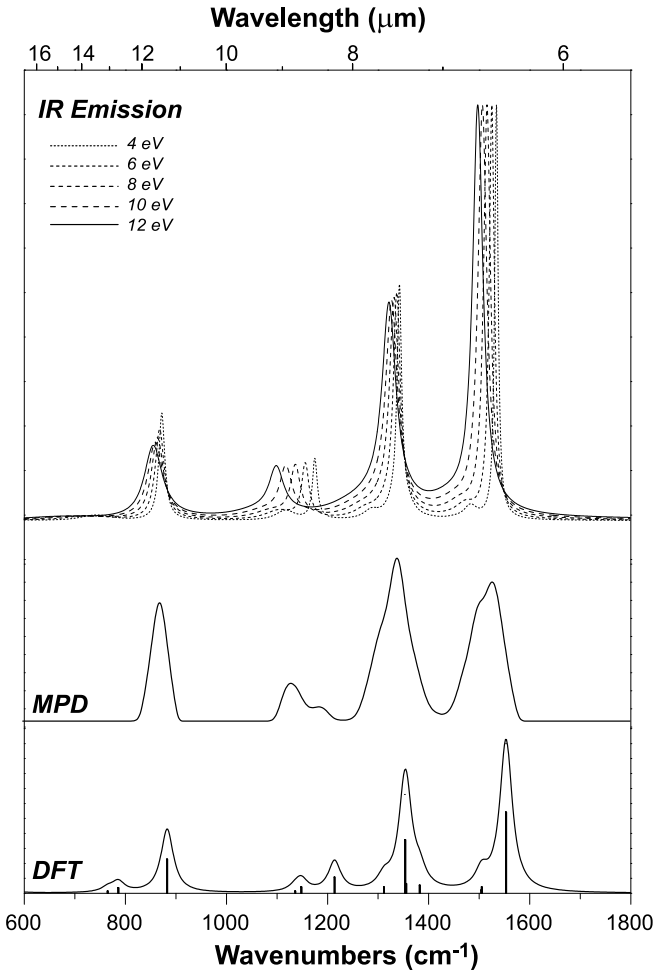

FIG. 6.—Computer simulations of the IRE spectrum (for different levels of UV excitation) and of the MPD spectrum of the coronene cation. Calculations are based on the same molecular parameters, i.e., the scaled DFT spectrum shown at the bottom (Langhoff 1996) and experimental anharmonicity data for neutral coronene (Joblin et al. 1995).

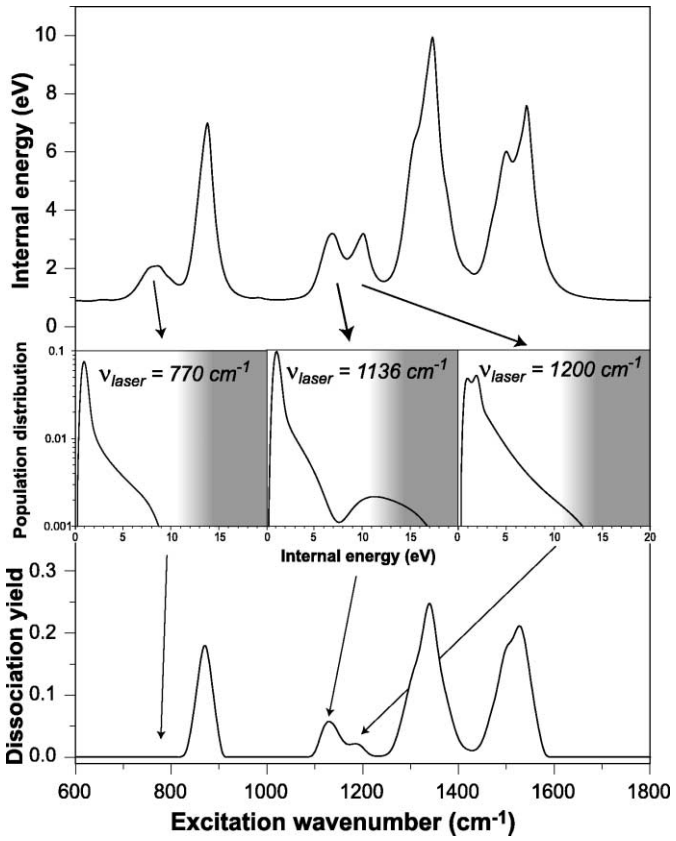

FIG. 7.—Multiple-photon excitation (*upper trace*) and corresponding multiple-photon dissociation spectrum (*lower trace*) for cationic coronene. The insets show the internal energy distribution at three different excitation wavelengths, where the gray shading represents the dissociation probability according to Arrhenius' law.

1973) and the scaling factor C was omitted. The final spectra were normalized to facilitate easy comparison of the spectra calculated for different UV excitation energies, which are shown in the top panel of Figure 6.

5.2. *MPD Model*

To estimate the internal energy distribution as a function of excitation wavelength, a mathematical model has previously been presented (von Helden et al. 1999; van Heijnsbergen et al. 2000; Oomens et al. 2001b). This model numerically evaluates a set of coupled differential equations describing the level populations of an anharmonic vibrational ladder coupled to a thermal bath of background states. In the top panel of Figure 7, the calculated multiple-photon excitation (MPE) spectrum of the coronene cation is shown for a laser fluence of 20 J cm^{-2} and a 4 cm^{-1} bandwidth. A spatial intensity distribution according to a Gaussian beam profile was taken into account for the infrared laser. In order to estimate the dissociation yield, the dissociation threshold of the coronene cation was taken to be 12 eV ($k_{\rm diss} = 10^4$ s^{-1}; Jochims et al. 1999). For large molecular systems, it is reasonable to assume that the rate of dissociation as a function of internal energy follows Arrhenius' law (Jochims et al. 1994, 1999), which was implemented in the model as

$$k_{\rm diss}(E) \approx \nu \exp[-E_{\rm diss}/kT(E)] \approx \exp[A - B/E(T)]\,, \quad (7)$$

where effective parameters A and B were determined from the data of Jochims et al. (1999). The dissociation rate was then integrated over the experimental time window to give the dissociation yield. The thus obtained MPD spectrum is plotted in the bottom panel of Figure 7.

It is instructive to compare the internal energy as a function of laser wavelength to the dissociation yield as a function of laser wavelength—representing the actual observable MPD spectrum—because it illustrates the nonlinearity of the MPD process. Let us focus on the three weak bands near 770, 1136, and 1200 cm^{-1}. As seen from the MPE spectrum, similar excitation energies are attained at these three laser frequencies. However, it is important to note that the internal energy plotted here is the *average* internal energy, which does not give any information on the distribution of internal energy. As we plot the internal energy distributions at the three different laser frequencies (see the insets in Fig. 7), subtle differences are observed that have a large impact on the actual MPD spectrum. The energy distribution at 1136 cm^{-1} is seen to have a small bump in the high-energy tail, which is above the dissociation threshold (*shaded area*) and therefore will undergo dissociation. At a laser frequency of 1200 cm^{-1}, a much smaller

fraction of the molecules reach an energy high enough to undergo dissociation, despite the fact that the average energy is not much different from excitation at 1136 cm^{-1}. Finally, at 770 cm^{-1}, the number of molecules reaching energies beyond the dissociation threshold is practically zero and no MPD signal is expected.

The differences in the shape of the internal energy distribution curve are a direct result of the nonlinear behavior of the multiple-photon absorption process. As the laser is in resonance with an allowed transition in the ion, multiple-photon absorption occurs, thereby heating up the ion and thus gradually shifting the band away from the laser frequency. This eventually decreases the efficiency of further excitation and results in a characteristic internal energy distribution, depending on laser bandwidth and fluence and on the mode-specific anharmonicity parameters. In addition, in the case in which there is another absorption band slightly to the blue (as is the case for the 1147 cm^{-1} mode), this band may gradually shift *into* resonance, especially for the hottest molecules in the ensemble. They may then undergo a second burst of multiple-photon absorption and reach internal energies beyond the dissociation threshold. In fact, the bump in the high-energy tail of the population distribution for laser excitation at 1136 cm^{-1} is exactly due to this process.

5.3. *Comparison of IRE and MPD*

Further study of the computer simulations in Figure 6 clearly shows that both the IRE (*top panel*) and the MPD (*middle panel*) processes cause a substantial "deformation" of the linear spectrum (*bottom panel*; linear absorption data from a scaled DFT calculation of Langhoff 1996 convoluted with a 30 cm^{-1} Lorentzian line shape). The influence of different anharmonicities for the different modes can be clearly seen, e.g., from the relative intensities of the 1553 and 1353 cm^{-1} bands. The intensity ratio in the MPD spectrum has reversed with respect to the DFT-calculated spectrum because of the twice as high anharmonic shift of the 1553 cm^{-1} band. In the IRE spectrum, however, the 1553 cm^{-1} band has even gained in intensity relative to the 1353 cm^{-1} band, as a consequence of the emission rate being proportional to the square of the frequency (see eq. [4]).

From the above discussion of the MPD process, it may be concluded that there is no straightforward way to relate the MPD and IRE spectra. As mentioned before, MPD relies on a monochromatic laser interaction, whereas IRE is fundamentally polychromatic. Nevertheless, from a close inspection of the spectra in Figure 6, it is seen that, depending on the level of excitation assumed for the emission spectrum, the MPD and IRE spectra may be rather close in terms of line width and redshift. This is mainly due to the fact that the two processes operate in roughly the same internal energy interval, since they are governed by the UV excitation level that lies roughly between 5 and 13.6 eV for IRE and by the dissociation threshold located roughly between 6 and 14 eV for MPD. One could therefore argue that MPD spectra may be used as an approach to interstellar emission spectra without explicit knowledge of anharmonicity parameters.

Finally, we note that in a true sample of interstellar coronene cations, it is likely that a distribution of different excitation energies occurs depending on the UV/visible absorption profile of the coronene cation convoluted with the spectral distribution of the interstellar UV field. Therefore, the true interstellar emission spectrum is likely represented by a corresponding average over the emission profiles calculated for individual excitation energies. Hence, the bandwidth observed in interstellar spectra is likely somewhat larger than those shown for the individual curves in Figure 6.

6. ASTROPHYSICAL IMPLICATIONS

In an attempt to make a meaningful comparison between the UIR spectrum and the different laboratory data, a composite spectrum has been generated based on available MIS and MPD data. Comparison is made with the *Infrared Space Observatory* (*ISO*) short-wavelength spectrometer (SWS) recorded UIR spectrum from the ionization ridge region of the M42 nebula in the Orion constellation, which is known for its high degree of ionization (Bregman et al. 1989). This ridge, known as the Orion Bar, forms the interface between an H II region irradiated by the Trapezium stars and an H I region molecular cloud. Only PAH species for which both MIS and MPD data are available have been included to be able to compare results from these two experimental methods. Figure 8 shows the composite spectrum of cationic phenanthrene, anthracene, pyrene, and coronene.

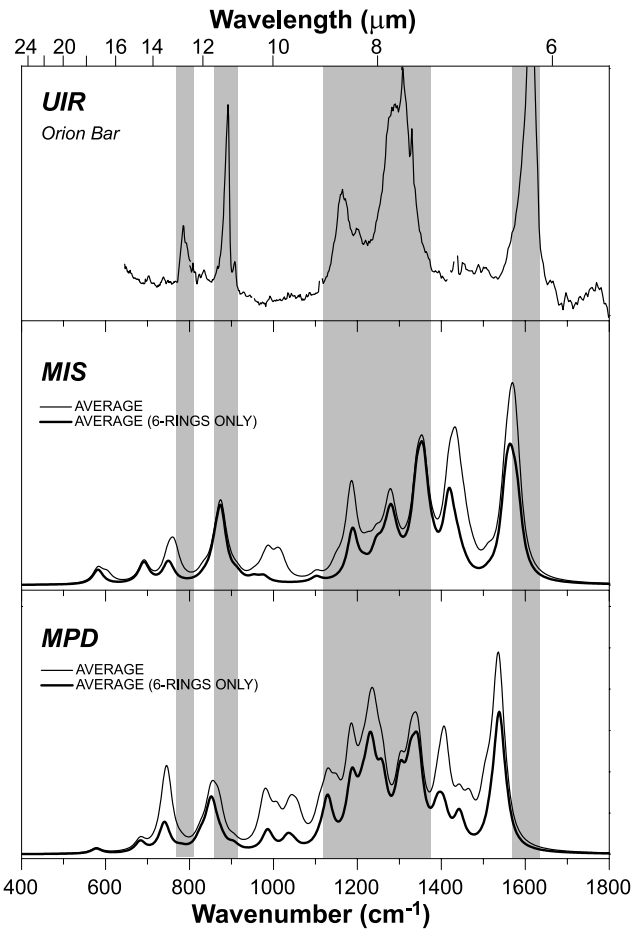

FIG. 8.—Experimental spectra of different cationic PAHs added for MIS and MPD methods and compared to the emission spectrum observed by *ISO* SWS from the Orion Bar region. *Thick line*: phenanthrene, anthracene, pyrene, coronene; *thin line*: phenanthrene, anthracene, pyrene, coronene, fluorene, fluoranthene.

Additionally, the spectrum including the five-membered ring species fluorene and fluoranthene is shown (*thin line*). In the composite spectra, all species were given equal weight and intensities were normalized to one for each of the species individually. To facilitate easy comparison of laboratory and interstellar spectra in Figure 8, the areas representing main UIR features have been shaded.

We realize that the chosen collection of ionic PAHs is a fairly poor representation of interstellar PAHs because the PAHs are relatively small, only a limited number of PAHs and only (singly) charged PAHs are included, etc. Using a more extensive spectral database, several fairly successful attempts to reproduce the UIR spectrum as closely as possible have been reported (Allamandola et al. 1999; Hudgins & Allamandola 1999a; Peeters et al. 2002), but this has not been the objective of this study. Nonetheless, it may be noted that in terms of overall relative spectral intensities, the agreement between the UIR spectrum from the ionization ridge in Orion and the composite experimental spectrum of ionic species only is not bad at all given the very rough comparison made here. In the following, we focus on some of the conclusions of § 4, which may have interesting astrophysical implications.

In both composite laboratory spectra, the CC stretching modes of the different species nicely line up to give a strong band near 1565 cm^{-1} in the MIS spectrum and near 1535 cm^{-1} in the MPD spectrum. As mentioned previously, in the in-plane CH bending region, a more diffuse spectral structure is formed by co-addition of the spectra of the individual species, which show more scattering in this region. Interestingly, in the UIR spectrum, the 6.2 μm band corresponding to the CC stretching modes appears as a relatively narrow feature ($\Delta\nu \approx 35$ cm^{-1}), whereas the 7.7 μm feature is at least a factor of 2 broader. In fact, high-resolution observations with the SWS spectrograph on board *ISO* recently revealed that this emission feature is a composite of several components, of which the relative intensities vary from source to source (Peeters et al. 2002). Moreover, including the weaker feature at 8.6 μm, emission is observed throughout the 1125–1375 cm^{-1} range, covering most of the CH in-plane bending modes in the laboratory spectra.

Another interesting observation is the consistent redshift of observed CC stretching modes with respect to the interstellar 6.2 μm band (1613 cm^{-1}), confirming recent observations (Hudgins & Allamandola 1999a; Peeters et al. 2002). In the MIS data the average position of the CC stretching band falls at 1568 cm^{-1} and, as a consequence of anharmonic shifting, at 1536 cm^{-1} in the average MPD spectrum. The calculations on the emission spectrum of the coronene cation suggest that anharmonicity causes a redshift to an extent at least in between the MPD and MIS data, so that the discrepancy between interstellar and laboratory spectra amounts to about 60 ± 15 cm^{-1}, or about 3.8%. According to Hudgins & Allamandola (1999a), this problem may be overcome by the introduction of larger cationic PAHs, although recently Peeters et al. (2002) reported that the gradual blueshift with increasing PAH size comes to an end around $n_C = 40$. It was also suggested in recent literature that a slight blueshift of the CC stretching mode could be induced by incorporation of a nitrogen atom in one of the benzenoid rings (Peeters et al. 2002) or by ionic PAHs with a closed-shell electronic structure formed from, e.g., (de)hydrogenated PAHs (Hudgins, Bauschilcher, & Allamandola 2001). In this context, it may also be interesting to mention ionic PAH metal atom adducts, although van Heijnsbergen et al. (2002) recently reported the observation of a redshifted CC stretching mode in V^+-benzene.

In terms of band positions, there is a poor match between interstellar and laboratory spectra in the CH out-of-plane bending region (600–900 cm^{-1}), which is likely due to the absence of solo CH species in the experimental samples. However, in terms of line widths, comparison of the Orion Bar spectrum with the observations of Figure 5 possibly points to an interesting conclusion. A general comparison of the MPD spectra of the various PAH ions showed consistently smaller line widths in the CH out-of-plane bending region with respect to the bands in the shorter wavelength range, and it was suggested that this is possibly due to anharmonicities being generally smaller for these modes. Indeed, the 11.3 μm emission band from the Orion Bar as shown in Figure 8 has a line width of only $\approx$15 cm^{-1}, which is a factor of 2 lower than for the 6.2 μm band. Theoretical anharmonicity parameters would be of great value to verify these arguments.

Close inspection of the composite laboratory spectra in Figure 8 shows that the main effect of excluding the five-membered ring species fluorene and fluoranthene (*thin line*) is to reduce the intensity in the spectral ranges around 1000 and around 1425 cm^{-1}. The absence of (strong) bands in these regions in the interstellar spectrum may then lead to the conclusion that such five-membered ring species are uncommon in the ISM. We note, however, that weak bands around 10 μm (1000 cm^{-1}) have been reported in emission spectra from certain sources, e.g., the nebula around NGC 1333 SVS 3 (Joblin et al. 1996; Sloan et al. 1999), the post-AGB star HR 4049, and the planetary nebulae NGC 7027 and IRAS 21282+5050 (Beintema et al. 1996).

7. DISCUSSION

Comparison of experimental methods.—Four different experimental techniques to obtain infrared spectra of ionic PAHs have been presented in § 2, and their results have been compared in § 3. Here we try to compare these techniques and answer the question of which technique is more suitable to unravel the astronomical observations. In Table 4, the most important experimental parameters are summarized, and it can be immediately seen that the different techniques can be quite complementary.

Both MIS and VDW techniques involve simple one-photon absorption processes and therefore represent linear absorption spectra, as opposed to MPD and IRE, which

TABLE 4
PARAMETERS FOR DIFFERENT EXPERIMENTAL METHODS

Parameter	MIS	MPD	VDW	IRE
Line width (cm^{-1})	1	30	5[a]	20 nm[b]
Temperature (K)	10	300	30	300
Gas phase	No	Yes	Yes	Yes
Linear	Yes	No	Yes	No
Mass selective	No	Yes	Yes	No
Emission/Absorption	A	A	A	E
PAH number[c]	17	11	4	1

[a] Determined by the laser bandwidth.
[b] Corresponds to 20 cm^{-1} at $\lambda = 10$ μm.
[c] Number of experimental spectra reported to date.

rely on multiple-photon absorption and emission, respectively. Therefore, the effects of anharmonicity are implicitly present in the spectra obtained with the latter two techniques, as is of course the case for the interstellar emission spectra (Barker et al. 1987). It should be noted that anharmonicity is implemented differently in absorption and emission processes so that, as expected, the IRE spectrum should give a result that is closest to the interstellar spectra.

However, IRE has proven to be an extremely difficult technique to record PAH cation spectra, and thus far only the infrared spectrum of cationic pyrene has been reported (Kim et al. 2001). On the other hand, if molecular anharmonicity parameters were known, it would be straightforward to generate an infrared emission spectrum from linear absorption data obtained from, e.g., the MIS spectrum. However, for the majority of (ionic) PAHs, no reliable anharmonicity data are available. The MPD method may be considered as an alternative: it has proven to be an efficient method for obtaining cationic PAH spectra in which the effects of anharmonicity are automatically included, although not exactly in the way they are implemented in an emission spectrum.

This brings about the issue of experimental complexity, which could roughly be estimated for the different techniques as the inverse of the number of PAH ion spectra published (see Table 4). Clearly, MIS is experimentally easiest to set up since the main components are a cryostat and an IR spectrometer, which are standard laboratory equipment nowadays. The MPD and VDW spectra were recorded using a free electron laser, which causes these techniques to not be generally applicable. However, the advance of new laser sources might change this in the near future. For instance, in the 3 μm range, laser sources based on parametric oscillators are now available, which can be used to obtain VDW spectra (Dopfer et al. 2002). Here we may also mention recent advances in IR-induced threshold ionization techniques making use of parametric oscillators (Fujii et al. 1999) or difference frequency generation (Fujii et al. 1997; Gerhards et al. 1998) in the 3 μm range. Application of MPD techniques (on covalently bound species) requires fairly high photon fluxes, and besides the FEL, only experiments using CO_2 lasers have been reported (Peiris et al. 1993). Their limited tuning range makes these lasers obsolete, however, for investigations relevant to the UIRs.

With the possibilities and limitations of each of these techniques in mind, one could address the question how to obtain experimental spectra of astrophysically relevant PAH-related compounds, such as large PAH ions, multiply charged PAHs, and hydrogen-deficient or fragmented PAHs. Thus far, as is clearly borne out by Table 1, the largest ionic PAHs were spectroscopically investigated using MIS (Bakes et al. 2001b). Using MPD, it has been shown that at least PAHs up to the size of coronene can be studied (Oomens et al. 2001b). However, it is known that because of the increasing number of vibrational degrees of freedom, the total energy that needs to be deposited in a molecule to induce dissociation scales approximately linearly with PAH size (Jochims et al. 1994, 1999). Moreover, in the absence of sufficiently high molecular symmetry, spectral congestion may become problematic, especially for MPD spectroscopy of these species. Because of the vibrational cooling in the molecular beam, VDW spectroscopy may be a good candidate to study these large PAH ions in the gas phase, if one succeeds in getting these extremely low vapor pressure species in the beam. Availability of high-temperature pulsed nozzles or stable laser desorption instruments is an important requirement here.

For the study of hydrogen-deficient and fragmented PAHs, it appears to be necessary to use a mass-selective technique. Application of ion traps, as used in the MPD experiments, allows one to isolate certain fragment masses prior to IR dissociation. In our opinion, such MS-MS techniques have the highest potential for the study of these PAH fragment ions. As an example, we recently recorded the IR spectrum of the benzoyl cation, $C_6H_5CO^+$, as a fragment of the benzoic acid cation (Oomens et al. 2003). The possible importance of such closed-shell ionic species under astrophysically relevant conditions was recently pointed out by Hudgins et al. (2001).

Multiply charged species may be of importance in regions of the ISM with strong UV irradiation (Bakes et al. 2001a, 2001b). To date, laboratory IR spectra of such species have not been reported. It should be noted that double ionization of relatively small PAHs is highly unlikely, and, therefore, some of the arguments mentioned for large PAHs apply here as well. In MIS, it may be extremely difficult to distinguish multiply charged from singly charged species using correlation measurements that are routinely used to differentiate between cationic, anionic, and neutral species. However, using mass-selective techniques, the charge state can be easily determined, and, therefore, we believe these techniques to be most promising for multiply charged PAHs at this moment.

Anharmonicity parameters.—On several occasions throughout this paper, the importance of accurate molecular anharmonicity parameters has been mentioned. From an astrophysical point of view, close inspection of the UIR spectrum reveals a red tail for most of the interstellar bands, which is believed to be due to anharmonic shifting in the highly excited species, and therefore, accurate knowledge of these parameters is desired. Interestingly, the 12.7 μm band is often seen to possess a blue tail, as can also be discerned in Figure 8.

From a comparison of linear absorption data (MIS and VDW) with multiple-photon absorption (MPD) or emission (IRE) data, anharmonicity parameters can in principle be extracted using an appropriate mathematical model. In § 4, we have shown that, in general, consistent redshifts can be found from a comparison of MIS and MPD data. In § 5, it was suggested that MPD data could serve as an approach to interstellar emission spectra without explicit knowledge of anharmonic parameters, although the multiple-photon excitation and emission processes are fundamentally different.

In an attempt to estimate anharmonicity parameters for an individual ion, we compare the VDW and MPD spectra for cationic naphthalene in Figure 9. Using the line positions of the linear VDW spectrum (Piest et al. 1999), the line intensities from the DFT calculations, and the model described in § 5.2, an MPD spectrum has been generated (third trace) as close as possible to the actual experimental MPD spectrum (Oomens et al. 2000) shown in the second trace. This method based on "visual fitting" results in anharmonicity parameters for each of the observed bands in the spectrum, as listed in Table 5. A dissociation threshold of 7 eV (Jochims et al. 1994), a laser fluence of 20 J cm^{-2}, and a laser bandwidth of 4 cm^{-1} are assumed.

Several tests of the model show that band positions are relatively insensitive to variations in laser fluence and

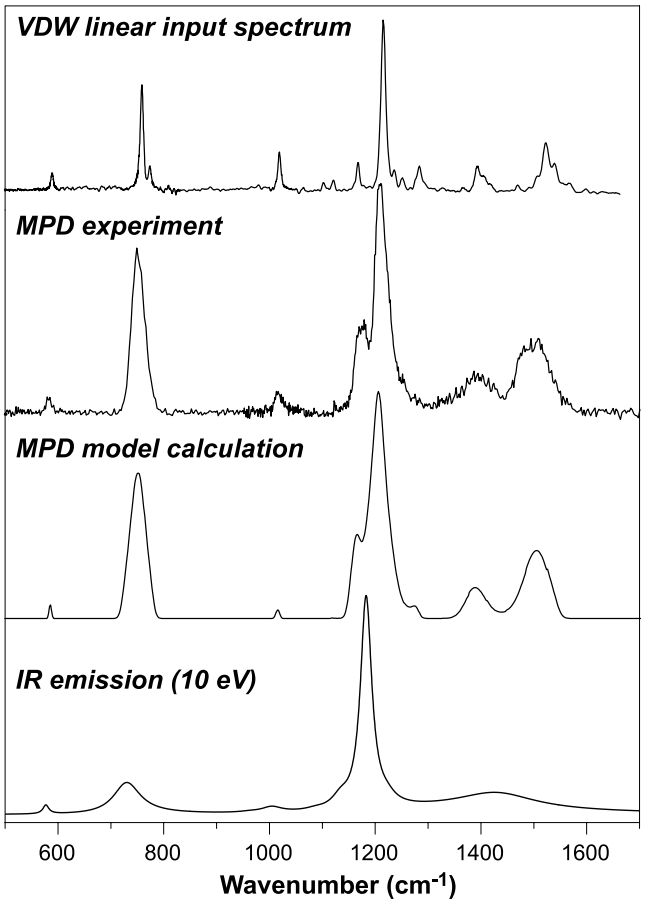

FIG. 9.—Application of MPD and IRE models to the naphthalene cation spectrum. The upper two traces show the linear spectrum as obtained by dissociation of the VDW complex (Piest et al. 1999) and the MPD spectrum (Oomens et al. 2000), respectively. Using the MPD model and the VDW data, the experimental MPD spectrum is simulated (*lower trace*), resulting in the parameters listed in Table 5. Subsequently, these parameters are used as input to the IRE model to generate an emission spectrum for an excitation energy of 10 eV, as shown in the lower trace.

TABLE 5

ANHARMONIC PARAMETERS DETERMINED FOR THE NAPHTHALENE CATION

Frequency[a] (cm^{-1})	I[b] ($\times 10^{-17}$cm)	a (cm^{-1})	b (cm^{-1})
589	0.13	−0.1	0.05
759	1.88	−0.3	0.3
1001	0.03	−0.5	0.3
1019	0.18	−0.2	0.3
1121	0.05	−0.5	0.3
1168	0.30	−0.5	0.3
1215	3.57	−0.5	0.2
1284	0.15	−1.0	0.3
1393	0.48	−1.3	2.6
1394	0.33	−1.3	2.6
1523	1.41	−2.0	1.8
1539	0.50	−2.0	1.6

[a] Taken from linear VDW spectrum of Piest et al. 1999.
[b] Taken from DFT calculation.

bandwidth, whereas the dependence on the anharmonicity a-parameter is strong, giving good confidence in the values in Table 5. However, it should be noted that a deviation in the dissociation threshold shifts the entire spectrum by a few cm^{-1} and, moreover, there likely exists some cross-correlation between parameters in Table 5. It should also be mentioned that anharmonic shift parameters substantially smaller than 0.4 cm^{-1} per quantum are probably inaccurate, since this represents an approximate lower limit on the observations. However, we believe that the anharmonicity parameters determined here represent at least good relative values. The observations made in § 4 that anharmonic shifts are in general larger in the CC stretching and in-plane CH bending range than in the CH out-of-plane bending range are quantitatively confirmed by the parameters reported in Table 5.

The derived anharmonicity parameters can now be used to calculate the emission spectrum using the model of § 5.1. For an excitation energy of 10 eV, this results in the spectrum given by the lower trace in Figure 9. The bands near the blue end of the spectrum are seen to merge almost completely because of the relatively large anharmonic shift and broadening parameters, whereas the main line in the spectrum, which possesses very small anharmonic parameters, retains a fairly narrow shape and therefore appears to become more prominent relative to the other bands in the spectrum. In general, this example illustrates the dramatic effects of vibrational anharmonicity on multiple-photon spectra.

Finally, we note once more that DFT-based predictions of anharmonicity parameters would be very helpful in supporting these preliminary experimental data. Moreover, they would be a very useful extension to the large amount of available calculated harmonic spectra of (ionic) PAHs, particularly in view of a detailed analysis of the UIR spectrum. Although anharmonic potentials have been calculated for smaller molecules (see, e.g., Martin et al. 1995; Miani et al. 2000; Van-Oanh, Parneix, & Bréchignac 2002), little or no such calculations have thus far been reported for PAHs.

8. SUMMARY

The available experimental infrared spectroscopic data on cationic PAHs, mainly based on four different experimental methods, have been analyzed and compared. More than 80% of the data rely on MIS and MPD experiments, representing linear and multiple-photon absorption data, respectively. Using a mathematical model for multiple-photon absorption and comparing linear and multiple-photon absorption data, we show that it is possible to retrieve anharmonic parameters for the different vibrational bands of cationic naphthalene. Such parameters are still largely unknown for the class of molecules (and molecular ions) under discussion here, yet they are important in modeling interstellar emission spectra. Since both multiple-photon MPD as well as linear MIS spectra are available for various ionic PAH species (see Fig. 3), their anharmonicity parameters can in principle be estimated, and this will be subject of further study.

Although multiple-photon absorption and infrared emission are fundamentally different processes, vibrational anharmonicity leads to similar redshifts in MPD and IRE spectra, particularly when a similar range of internal energies is considered, which normally is the case for stable PAH ions. A comparison of the various PAH ion spectra

shows that there is a general trend for the effects of anharmonicity to be more pronounced in the CC stretching range than in the CH out-of-plane bending range. Possible manifestations of this trend in the interstellar spectra have been discussed.

This work is part of the research program of FOM, which is financially supported by the Nederlandse Organisatie voor Wetenschappelijk Onderzoek (NWO).

REFERENCES

Allamandola, L. J., Hudgins, D. M., & Sandford, S. A. 1999, ApJ, 511, 115L
Allamandola, L. J., Tielens, A. G. G. M., & Barker, J. R. 1985, ApJ, 290, L25
———. 1989, ApJS, 71, 733
Bakes, E. L. O., Tielens, A. G. G. M., & Bauschlicher, Jr, C. W. 2001a, ApJ, 556, 501
Bakes, E. L. O., Tielens, A. G. G. M., Bauschlicher, Jr, C. W., Hudgins, D. M., & Allamandola, L. J. 2001b, ApJ, 560, 261
Bakker, J. M., Satink, R. G., von Helden, G., & Meijer, G. 2002, Chem. Phys., 4, 24
Banisaukas, J., et al. 2003, J. Phys. Chem., 107, 782
Barker, J. R., Allamandola, L. J., & Tielens, A. G. G. M. 1987, ApJ, 315, L61
Bauschlicher, C. W., Jr. 2002, ApJ, 564, 782
Bauschlicher, C. W., Jr., & Bakes, E. L. O. 2000, Chem. Phys., 262, 285
Bauschlicher, C. W., Jr., Hudgins, D. M., & Allamandola, L. J. 1999, Theor. Chem. Accounts, 103, 154
Becke, A. D. 1988, Phys. Rev. A, 38, 3098
Beintema, D. A., et al. 1996, A&A, 315, L369
Boulanger, F., Boisssel, P., Cesarsky, D., & Ryter, C. 1998, A&A, 339, 194
Bregman, J. D., Allamandola, L. J., Tielens, A. G. G. M., Geballe, T. R., & Witteborn, F. C. 1989, ApJ, 344, 791
Brenner, J. D., & Barker, J. R. 1992, ApJ, 388, L39
Cherchneff, I., & Barker, J. R. 1989, ApJ, 341, L21
Colangeli, L., Mennella, V., Baratta, G. A., Bussoletti, E., & Strazzulla, G. 1992, ApJ, 396, 369
Cook, D. J., & Saykally, R. J. 1998, ApJ, 493, 793
Cook, D. J., Schlemmer, S., Balucani, N., Wagner, D. R., Harrison, J. A., Steiner, B., & Saykally, R. J. 1998, J. Phys. Chem., 102, 1465
DeFrees, D. J., Miller, M. D., Talbi, D., Pauzat, F., & Ellinger, Y. 1993, ApJ, 408, 530
Dopfer, O., Olkhov, R. V., & Maier, J. P. 1999, J. Chem. Phys., 111, 10,754
Dopfer, O., Roth, D., & Maier, J. P. 2002, J. Am. Chem. Soc., 124, 494
Draine, B. T., & Li, A. 2001, ApJ, 551, 807
Dunbar, R. C. 2000, Int. J. Mass Spectrom. Ion Processes, 200, 571
Ekern, S. P., Marshall, A. G., Szczepanski, J., & Vala, M. 1998, J. Phys. Chem., 102, 3498
Flickinger, G. C., Wdowiak, T. J., & Gomez, P. L. 1991, ApJ, 380, L43
Frisch, M. J., et al. 1998, Gaussian 1998 Revision A7 (Pittsburgh: Guassian Inc.)
Fujii, A., Fujimaki, E., Ebata, T., & Mikami, N. 1999, Chem. Phys. Lett., 303, 289
———. 2000, J. Chem. Phys., 112, 6275
Fujii, A., Iwasaki, A., Ebata, T., & Mikami, N. 1997, J. Phys. Chem., 101, 5963
Genzel, R., et al. 1998, ApJ, 498, 579
Gerhards, M., Schiwek, M., Unterberg, C., & Kleinermanns, K. 1998, Chem. Phys. Lett., 297, 515
Gillett, F. C., Forrest, W. J., & Merrill, K. M. 1973, ApJ, 183, 87
Henning, Th., Klein, R., Launhardt, R., Lemke, D., & Pfau, W. 1998, A&A, 332, 1035
Hillenbrand, S., Zhu, L., & Johnson, P. 1991, J. Chem. Phys., 95, 2237
Hony, S., Van Kerckhoven, C., Peeters, E., Tielens, A. G. G. M., Hudgins, D. M., & Allamandola, L. J. 2001, A&A, 370, 1030
Hudgins, D. M., & Allamandola, L. J. 1995a, J. Phys. Chem., 99, 3033
———. 1995b, J. Phys. Chem., 99, 8978
———. 1997, J. Phys. Chem., 101, 3472
———. 1999a, ApJ, 513, L69
———. 1999b, ApJ, 516, L41
Hudgins, D. M., Bauschlicher, C. W., Jr., & Allamandola, L. J. 2001, Spectrochim. Acta, 57, 907
Hudgins, D. M., Bauschlicher, C. W., Jr., Allamandola, L. J., & Fetzer, J. C. 2000, J. Phys. Chem., 104, 2655
Hudgins, D. M., Sandford, S. A., & Allamandola, L. J. 1994, J. Phys. Chem., 98, 4243
Jahn, H. A., & Teller, E. 1937, Proc. Astron. Soc. Australia, 161, 220
Joblin, C., Abergel, A., Bregman, J., d'Hendecourt, L., Heras, A. M., Jourdain de Muizon, M., Pech, C., & Tielens, A. G. G. M. 2000, in *ISO* beyond the Peaks, ed. A. Salama, M. F. Kessler, K. Leech, & B. Schulz (ESA SP-456; Noordwijk: ESA), 49
Joblin, C., Boissel, P., Léger, A., d'Hendecourt, L., & Défourneau, D. 1995, A&A, 299, 835
Joblin, C., d'Hendecourt, L., Léger, A., & Défourneau, D. 1994, A&A, 281, 923
Joblin, C., Tielens, A. G. G. M., Geballe, T. R., & Wooden, D. H. 1996, ApJ, 460, L119
Jochims, H. W., Baumgärtel, H., & Leach, S. 1999, ApJ, 512, 500
Jochims, H. W., Rühl, E., Baumgärtel, H., Tobita, S., & Leach, S. 1994, ApJ, 420, 307
Keszthelyi, T., Balakrishnan, G., Wilbrandt, R., Yee, W. A., & Negri, F. 2000, J. Phys. Chem., 104, 9121
Kim, H.-S., Wagner, D. R., & Saykally, R. J. 2001, Phys. Rev. Lett., 86, 5691
Kurtz, J. 1992, A&A, 255, L1
Langhoff, S. R. 1996, J. Phys. Chem., 100, 2819
Léger, A., d'Hendecourt, L., & Defourneau, D. 1989, A&A, 216, 148
Léger, A., & Puget, J. L. 1984, A&A, 137, L5
March, R. E., & Londry, F. A. 1995, in Practical Aspects of Ion Trap Mass Spectrometry, Vol. I: Fundamentals of Ion Trap Mass Spectrometry, ed. R. E. March & J. F. J. Todd (Boca Raton: CRC Press), 25
Martin, J. M. L., Lee, T. J., Taylor, P. R., & Francois, J. P. 1995, J. Chem. Phys., 103, 2589
Mattila, K., Lehtinen, K., & Lemke, D. 1999, A&A, 342, 643
Mattila, K., Lemke, D., Haikala, L. K., Laureijs, R. J., Léger, A., Lehtinen, K., Leinert, C., & Mezger, P. G. 1996, A&A, 315, L353
Miani, A., Cané, E., Palmieri, P., Trombetti, A., & Handy, N. C. 2000, J. Chem. Phys., 112, 248
Moutou, C., Léger, A., & d'Hendecourt, L. 1996, A&A, 310, 297
Moutou, C., Verstraete, L., Sellgren, K., & Léger, A. 1999, in The Universe as Seen by *ISO*, ed. P. Cox (ESA SP-427; Noordwijk: ESA), 727
Müller-Dethlefs, K., & Schlag, E. W. 1991, Annu. Rev. Phys. Chem., 42, 109
Oepts, D., van der Meer, A. F. G., & van Amersfoort, P. W. 1995, Infrared Phys., 36, 297
Okumura, M., Yeh, L. I., Myers, J. D., Lee, Y. T. 1986, J. Chem. Phys., 85, 2328
Oomens, J., Bakker, J. M., Sartakov, B. G., Meijer, G., & von Helden, G. 2003, Chem. Phys. Lett., 367, 576
Oomens, J., Meijer, G., & von Helden, G. 2001a, J. Phys. Chem., 105, 8302
Oomens, J., Sartakov, B. G., Tielens, A. G. G. M., Meijer, G., & von Helden, G. 2001b, ApJ, 560, L99
Oomens, J., van Roij, A. J. A., Meijer, G., & von Helden, G. 2000, ApJ, 542, 404
Paul, W. 1990, Rev. Mod. Phys., 62, 531
Pauzat, F., Talbi, D., Miller, M. D., DeFrees, D. J., & Ellinger, Y. 1992, J. Phys. Chem., 96, 7882
Pech, C., Joblin, C., & Boissel, P. 2002, A&A, 388, 639
Peeters, E., Hony, S., Van Kerckhoven, C., Tielens, A. G. G. M., Allamandola, L. J., Hudgins, D. M., & Bauschlicher, C. W. 2002, A&A, 390, 1089
Peiris, D. M., Cheeseman, M. A., Ramanathan, R., & Eyler, J. R. 1993, J. Phys. Chem., 97, 7839
Perdew, J. P. 1986, Phys. Rev. B, 33, 8822
Piest, J. A., Oomens, J., Bakker, J., von Helden, G., & Meijer, G. 2001, Spectrochim. Acta, 57, 717
Piest, J. A., von Helden, G., & Meijer, G. 1999, ApJ, 520, L75
Russell, R. W., Soifer, B. T., & Willner, S. P. 1977, ApJ, 217, L149
Satink, R. G., Bakker, J. M., Meijer, G. M., & von Helden, G. 2002, Chem. Phys. Lett., 359, 163
Satink, R. G., Piest, H., von Helden, G., & Meijer, G. 1999, J. Chem. Phys., 111, 10750
Schlemmer, S., Cook, D. J., Harrison, J. A., Wurfel, B., Chapman, W., & Saykally, R. J. 1994, Science, 265, 1686
Schutte, W. A., Tielens, A. G. G. M., & Allamandola, L. J. 1993, ApJ, 415, 397
Shan, J., Suto, M., & Lee, L. C. 1991, ApJ, 383, 459
Shin, S. K., & Beauchamp, J. L. 1990, J. Am. Chem. Soc., 112, 2066
Sloan, G. C., Hayward, T. L., Allamandola, L. J., Bregman, J. D., DeVito, B., & Hudgins, D. M. 1999, ApJ, 513, L65
Stein, S. E., & Rabinovitch, B. S. 1973, J. Chem. Phys., 58, 2438
Szczepanski, J., Banisaukas, J., Vala, M., Hirata, S., Bartlett, R. J., & Head-Gordon, M. 2002, J. Phys. Chem., 106, 63
Szczepanski, J., Roser, D., Personette, W., Eyring, M., Pellow, R., & Vala, M. 1992, J. Phys. Chem., 96, 7876
Szczepanski, J., & Vala, M. 1993, ApJ, 414, 646
Szczepanski, J., Vala, M., Talbi, D., Parisel, O., & Ellinger, Y. 1993, J. Chem. Phys., 98, 4494
Vala, M., Szczepanski, J., Pauzat, F., Parisel, O., Talbi, D., & Ellinger, Y. 1994, J. Phys. Chem., 98, 9187
van Heijnsbergen, D., von Helden, G., Meijer, G., Maitre, P., & Duncan, M. A. 2002, J. Am. Chem. Soc., 124, 1562

van Heijnsbergen, D., von Helden, G., Sartakov, B., & Meijer, G. 2000, Chem. Phys. Lett., 321, 508
Van Kerckhoven, et al. 2000, A&A, 357, 1013
Van-Oanh, N.-T., Parneix, P., & Bréchignac, P. 2002, J. Phys. Chem., 106, 10144
Verstraete, L., et al. 2001, A&A, 372, 981
Verstraete, L., Puget, J. L., Falgarone, E., Drapatz, S., Wright, C. M., & Timmermann, R. 1996, A&A, 315, L337
von Helden, G., Holleman, I., Meijer, G., & Sartakov, B. 1999, Opt. Express, 4, 46
Willner, S. P., Soifer, B. T., Russell, R. W., Joyce, R. R., & Gillett, F. C. 1977, ApJ, 217, L121
Zhang, X., Pitts, J. D., Nadarajah, R., & Knee, J. L. 1997, J. Chem. Phys., 107, 8239
Zhu, L., & Johnson, P. 1991, J. Chem. Phys., 94, 5769